USGS
science for a changing world

Prepared in cooperation with the Albuquerque Bernalillo County Water Utility Authority

Land Subsidence and Recovery in the Albuquerque Basin, New Mexico, 1993–2014

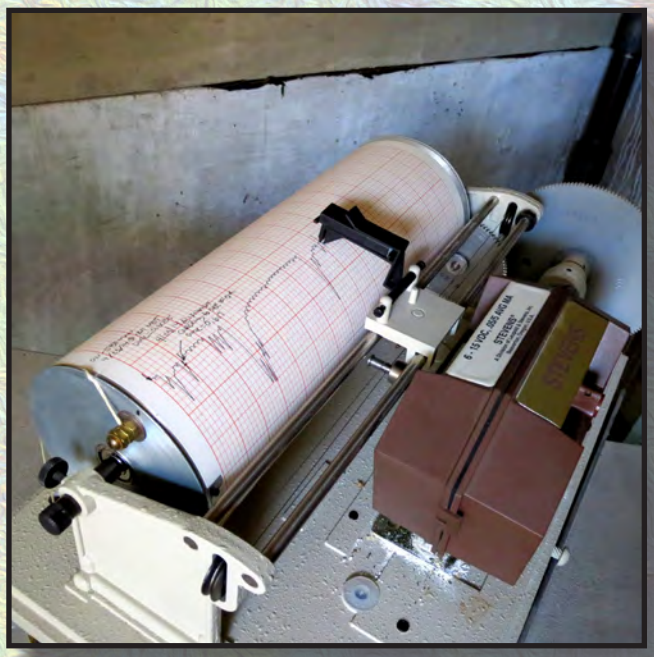

Scientific Investigations Report 2017–5057

U.S. Department of the Interior
U.S. Geological Survey

Cover. Photographs showing Stevens Chart Recorder at the Albuquerque extensometer:
Left photograph, collecting aquifer compaction data, and
Right photograph, quarterly maintenance on the extensometer.

Land Subsidence and Recovery in the Albuquerque Basin, New Mexico, 1993–2014

By Jessica M. Driscoll and Justin T. Brandt

Prepared in cooperation with the Albuquerque Bernalillo County Water Utility Authority

Scientific Investigations Report 2017–5057

U.S. Department of the Interior
U.S. Geological Survey

U.S. Department of the Interior
RYAN K. ZINKE, Secretary

U.S. Geological Survey
William H. Werkheiser, Acting Director

U.S. Geological Survey, Reston, Virginia: 2017

Suggested citation:
Driscoll, J.M., and Brandt, J.T., 2017, Land subsidence and recovery in the Albuquerque Basin, New Mexico, 1993–2014: U.S. Geological Survey Scientific Investigations Report 2017–5057, 31 p.,https://doi.org/10.3133/sir20175057.

ISSN 2328-0328 (online)

Contents

Figures

Tables

Conversion Factors

International System of Units to U.S. customary units

Multiply	By	To obtain
	Length	
centimeter (cm)	0.3937	inch (in.)
millimeter (mm)	0.03937	inch (in.)
meter (m)	3.281	foot (ft)
kilometer (km)	0.6214	mile (mi)
meter (m)	1.094	yard (yd)

Datum

Vertical coordinate information is referenced to the North American Vertical Datum of 1988 (NAVD 88).

Elevation, as used in this report, refers to distance above the vertical datum.

Abbreviations

ABCWUA	Albuquerque Bernalillo County Water Utility Authority
CGPS	Continuous Global Positioning System
ENVISAT	Environmental Satellite
GPS	Global Positioning System
InSAR	Interferometric Synthetic Aperture Radar
LSS	Land-subsidence survey
SAR	Synthetic Aperture Radar
SJCDWP	San Juan-Chama Drinking Water Project
USGS	U.S. Geological Survey

Land Subsidence and Recovery in the Albuquerque Basin, New Mexico, 1993–2014

By Jessica M. Driscoll and Justin T. Brandt

Abstract

The Albuquerque Bernalillo County Water Utility Authority (ABCWUA) drinking water supply was almost exclusively sourced from groundwater from within the Albuquerque Basin before 2008. In 2008, the San Juan-Chama Drinking Water Project (SJCDWP) provided surface-water resources to augment the groundwater supply, allowing for a reduction in groundwater pumping in the Albuquerque Basin. In 2013, the U.S. Geological Survey, in cooperation with the ABCWUA, began a study to measure and compare aquifer-system and land-surface elevation change before and after the SJCDWP in 2008. Three methods of data collection with different temporal and spatial resolutions were used for this study: (1) aquifer-system compaction data collected continuously at a single extensometer from 1994 to 2013; (2) land-surface elevation change from Global Positioning System (GPS) surveys of a network of monuments collected in 1994–95, 2005, and 2014; and (3) spatially distributed Interferometric Synthetic Aperture Radar (InSAR) satellite data from 1993 to 2010. Collection of extensometer data allows for direct and continuous measurement of aquifer-system compaction at the extensometer location. The GPS surveys of a network of monuments allow for periodic measurements of land-surface elevation change at monument locations. Interferograms are limited in time by lifespan of the satellite, orbital pattern, and data quality but allow for measurement of gridded land-surface elevation change over the study area. Each of these methods was employed to provide a better understanding of aquifer-system compaction and land-surface elevation change for the Albuquerque Basin.

Results do not show large magnitudes of subsidence in the Albuquerque Basin. High temporal-resolution but low spatial-resolution data measurements of aquifer-system compaction at the Albuquerque extensometer show elastic aquifer-system response to recovering groundwater levels. Results from the GPS survey of the network of monuments show inconsistent land-surface elevation changes over the Albuquerque Basin, likely because of the lack of significant change and the complexity of subsurface stratigraphy in addition to the spatial and temporal heterogeneity of groundwater withdrawals over the study period. Results from the InSAR analysis show areas of land-surface elevation increase after 2008, which could be attributed to elastic recovery of the aquifer system. The spatial extent to which elastic recovery of the aquifer system has resulted in recovery of land-surface elevation is limited to the in-situ measurements at the extensometer. Examination of spatially distributed InSAR data relative to limited spatial extent of the complex heterogeneity subsurface stratigraphy may explain some of the heterogeneity of land-surface elevation changes over this study period.

Introduction

Sustained groundwater withdrawals for municipal and agricultural uses in excess of recharge have resulted in aquifer-system compaction and resultant subsidence typically of a meter to several meters in alluvial basins in Arizona, California, and Nevada and as much as 9 meters (m) in the San Joaquin Valley, California (Galloway and others, 1999; Bell and others, 2002; Sneed and others, 2013, 2014). These studies and others (Hoffmann and others, 2001; Schmidt and Bürgmann, 2003) also show that groundwater-level recovery can result in reduced rates of subsidence or even uplift of the land surface.

The Albuquerque Bernalillo County Water Utility Authority (ABCWUA, 2009) has the responsibility of effectively managing the water supply for the greater Albuquerque metropolitan area, located in the Albuquerque Basin in north-central New Mexico (fig. 1). Water supply for the metropolitan areas within the Albuquerque Basin historically has been met nearly exclusively by groundwater withdrawals from the Santa Fe Group aquifer, resulting in water-level declines in the aquifer system (Bexfield and Anderholm, 2002; Falk and others, 2011). In 2008, the source of water for the city of Albuquerque was augmented with surface-water supplies from the San Juan-Chama Drinking Water Project (SJCDWP), allowing the ABCWUA to

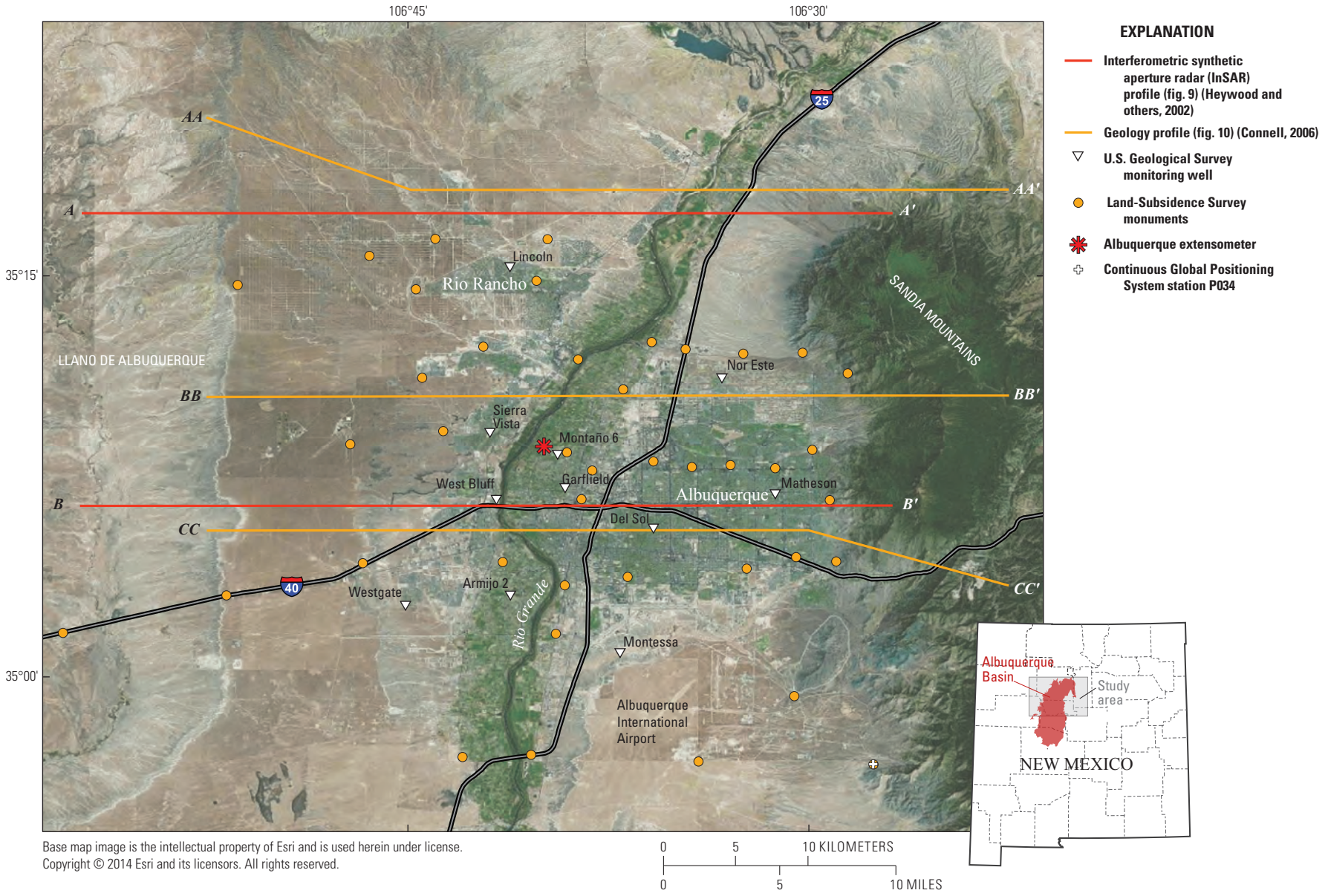

Figure 1. Location of the Albuquerque Basin study area.

withdraw less groundwater for water supply. This reduction of groundwater pumpage for municipal water supply resulted in subsequent groundwater-level recovery in some locations (Powell and McKean, 2014; Beman and Bryant, 2016). In 2013, the U.S. Geological Survey (USGS), in cooperation with the ABCWUA, began a study in the Albuquerque Basin to measure and compare these data with previous investigations of aquifer-system compaction and land-surface elevation change in the basin.

Purpose and Scope

The purpose of this report is to document and summarize the results of land subsidence and recovery in the Albuquerque Basin from 1993 to 2014. This report presents measurements and analyses of aquifer-system response (through in-situ measurements of aquifer-system compaction and land-surface elevation change) to changes in groundwater levels before and after the SJCDWP began to supply water to the customers served by the ABCWUA. Three methods of data collection and analysis with varying temporal and spatial resolutions were used for this study: (1) aquifer-system compaction data collected continuously at a single borehole extensometer from 1994 to 2013; (2) land-surface elevation change from Global Positioning System (GPS) surveys in 1994–95, 2005, and 2014; and (3) spatially distributed Interferometric Synthetic Aperture Radar (InSAR) satellite data from 1993 to 2010. This study uses these methods in order to (1) measure aquifer-system compaction over time, including analysis of trends in elastic and inelastic compaction; (2) measure the land-surface elevation for the existing benchmark network using a GPS survey in 2014; (3) measure vertical land-surface displacement using InSAR from 2003 to 2010, (4) compare new data measured for this study to data from previous studies on subsidence in the basin, and (5) compare these data with groundwater-levels in the basin, specifically before and after the start of the SJCDWP in 2008.

Description of the Study Area

The Albuquerque Basin is located in north-central New Mexico and extends approximately 160 kilometers (km) from north to south and varies between approximately 40 and 65 km west to east from the Llano de Albuquerque to the Sandia Mountains (fig. 1). The basin is defined as the extent of consolidated and unconsolidated Tertiary- and Quaternary-age deposits within the Rio Grande Rift Valley, which consists of a series of generally north-to-south trending structural basins (Thorn and others, 1993; McAda and Barroll, 2002). The basin is approximately bisected by the southward-flowing Rio Grande, the only perennial stream extending through the length of the basin.

The study area focuses on the unconsolidated deposits in the Albuquerque Basin within the Rio Grande Rift Valley, including the Albuquerque and Rio Rancho metropolitan areas, from the Llano de Albuquerque to the Sandia Mountains (fig. 1). A 20-percent population increase in the basin from 1990 to 2000 and a 22-percent increase from 2000 to 2010 may have resulted in an increased demand for water (Beman and Bryant, 2016). The majority of the population of New Mexico lives within this basin, and until 2008 water supply was almost exclusively provided through groundwater pumping. In 2008, the ABCWUA implemented the SJCDWP, which delivers water allocated to water users in New Mexico as part of the Upper Colorado River Compact (ABCWUA, 2009). The city of Albuquerque, through the ABCWUA, was able to reduce groundwater pumping by augmenting the water supply with surface water from the SJCDWP's interbasin transfer of water from the Colorado River Basin to the Rio Grande Basin. The cities of Albuquerque and Rio Rancho also have managed aquifer recovery projects using treated reclaimed water within their respective boundaries.

The Albuquerque Basin (fig. 1) is one of a series of physiographic basins within the Rio Grande Rift Valley. The Santa Fe Group is the dominant fill unit of the Albuquerque Basin (Hawley, 1994). The principal aquifer in the Albuquerque Basin groundwater system is the Santa Fe Group aquifer, which comprises deposits of middle Pleistocene to late Oligocene age and is divided into upper (from less than 300 to 460 m thick), middle (from 75 to 2,750 m thick), and lower (from less than 300 to 1,050 m thick) sections (Bartolino and Cole, 2002). The depth to water in the Santa Fe Group aquifer system varies widely from less than 1.5 m near the Rio Grande to more than 300 m west of Albuquerque (Bartolino and Cole, 2002; Connell, 2006; Beman and Bryant, 2016).

The stratigraphy of the Santa Fe Group is complex, with many units varying in thickness as well as lateral extent in the area. The majority of the thickness of the Santa Fe Group is sandy to silty in the Albuquerque Basin; however, there are more clay-rich components, such as the Atrisco Member (T_{ca}) of the Ceja Formation (T_c) (Bartolino and Cole, 2002; Connell, 2006). The Atrisco Member is described as a distinctive, laterally extensive, light yellowish-brown to yellowish-red, fine-grained, interbedded silty sand and clay unit with a thickness ranging from 85 to 100 m (Connell and others, 1998). There are also clay-sand, interbedded sequences within the Sierra Ladrones Formation (QT_{sa}, QT_{sp}), which overlie the Atrisco Member (Connell, 2006).

More deformation might be expected to occur where groundwater levels decline within a more compressible stratigraphic unit comprised of fine-grained (silt and clay) compared to relatively less compressible coarse-grained (sand and gravel) deposits (Galloway and others, 1999). The relatively clay-rich Atristco Member may then be the most likely formation in the Albuquerque Basin where compaction could occur because of the relatively more compressible, clay-rich composition, which is unique compared to the generally otherwise ubiquitous sand-rich composition of the Santa Fe Group. The fine-grained, interbedded sequences of the Sierra Ladrones Formation above the Atrisco Member would also be expected to be relatively susceptible to aquifer-system compaction; however, these deposits are less laterally extensive (Connell, 2006).

Groundwater generally enters the Albuquerque Basin groundwater system through contributions from upstream tributaries, mountain front recharge, surface-water/groundwater exchange with the Rio Grande, surface-water/groundwater exchange within the irrigated inner valley of the Rio Grande, and inflow from upgradient subsurface flow. Groundwater generally leaves the groundwater system through pumping from wells (though some of this reenters the groundwater system as return flow), seepage into the Rio Grande and (or) riverside drains, evapotranspiration, and subsurface outflow to the downgradient Socorro Basin to the south (Bartolino and Cole, 2002). The effect of pumping may cause outflow from the system to exceed inflow; the difference will be compensated by flows into the system from aquifer-system storage and (or) captured flows from other inflow sources, reduced outflow through evapotranspiration, stream/groundwater exchange, and subsurface groundwater flow (Konikow and Leake, 2014). Flows from aquifer-system storage cause groundwater levels to decline and may cause susceptible sediments in the aquifer system to compact and land subsidence to occur.

Mechanics of Pumping-Induced Land Subsidence

Land subsidence attributed to groundwater pumping occurs in many aquifer systems that are, at least in part, made up of unconsolidated fine-grained sediments that have undergone extensive groundwater development (Poland, 1984). The relation between changes in pore-fluid pressure and compression of the aquifer system is based on the principle of effective stress (Terzaghi, 1925),

$$\sigma_e = \sigma_T - p \tag{1}$$

where σ_e is the effective or intergranular stress,
σ_T is the total stress or geostatic load, and
p is the pore-fluid pressure.

The pore structure of a sedimentary aquifer system is supported by the granular skeleton of the aquifer system and the pore-fluid pressure of the groundwater that fills the intergranular pore space (Meinzer, 1928). If total stress remains constant and groundwater is withdrawn in quantities that result in reduced pore-fluid pressures [or equivalent heads (h) where $h=p/(\rho g)$, where ρ is the density and g is gravity] and water-level declines, the reduction of the pore-fluid-pressure support results in equivalent increases in the intergranular stress, or effective stress, on the skeleton. A change in effective stress deforms the skeleton—an increase in effective stress compresses it and a decrease in effective stress causes it to expand. The deformation may be elastic (recoverable) or inelastic (largely nonrecoverable) depending on the previous maximum stress exerted on the skeleton. The vertical component of this deformation sometimes results in compaction of the aquifer system and land subsidence. An aquifer-system skeleton that consists of primarily fine-grained sediments, such as silt and clay, tends to be much more compressible than one that consists primarily of coarse-grained sediments, such as sand and gravel. Inelastic compaction of coarse-grained sediment can generally be assumed to be negligible.

Aquifer-system deformation is elastic if the stress imposed on the skeleton is smaller than any previous effective stress (Leake and Prudic, 1988). The largest historical effective stress imposed on the aquifer system—sometimes the result of the lowest groundwater level—is the "preconsolidation stress." If the effective stress is greater than the preconsolidation stress, the pore structure of the granular matrix of the fine-grained sediments is rearranged; this new configuration results in a reduction of pore volume and, thus, inelastic compaction of the aquifer system. Furthermore, the compressibility of the fine-grained sediments constituting the aquitards (interbeds and confining units), and any resulting compaction under stresses greater than the preconsolidation stress, is inelastic and generally from 20 to more than 100 times greater than for stresses less than the preconsolidation stress (Riley, 1998).

Terzaghi's theory of hydrodynamic consolidation (1925) describes the delayed drainage and consolidation of compressible fine-grained sediments in response to decreased fluid pressures in the bounding sediments. For an aquifer-system skeleton with an appreciable thickness of fine-grained sediments, a significant part of the total compaction may be residual compaction. Residual compaction is compaction that generally occurs in thick aquitard layers while heads in the aquitard equilibrate with heads in the adjacent (above and below) aquifers (Riley, 1969). For a homogeneous aquitard bounded above and below by aquifers in which the head is lowered instantaneously and equally, a time constant (τ), the time required to attain about 93 percent of equilibration of head in the aquitard with heads in the aquifers, can be computed using

$$\tau = S'_s \left(b'/2\right)^2 / K'_v \tag{2}$$

where S'_s is the specific storage of the aquitard,
b' is the thickness of the aquitard, and
K'_v is the vertical hydraulic conductivity of the aquitard.

Compaction is governed by S'_s:

$$\begin{aligned} &S_{s'} = S_{s'_k} + S_{s'_w} = \gamma_w(\alpha' + n'\beta_w), \text{ where} \\ &S_{s'_k} = \gamma_w \alpha', \text{ and} \\ &S_{s'_w} = \gamma_w n' \beta_w \end{aligned} \tag{3}$$

where $S_{s'_k}$ is the skeletal specific storage,
$S_{s'_w}$ is the specific storage of water,
α' is the skeletal compressibility,
β_w is the fluid compressibility,
n' is porosity, and
γ_w is the specific weight of water.

Compaction can be computed for a change in effective stress ($\Delta\sigma_e$) caused by a change in fluid pressure (Δp) (equation 1 for $\Delta\sigma_T = 0$) using (Hoffmann and others, 2003):

$$\Delta b' = \frac{S_{s_k}' b_0' \, \Delta\sigma_e}{\gamma_w} = \frac{S_{s_k}' b_0' \, \Delta p}{\gamma_w} = S_{s_k}' b_0' \, \Delta h \qquad (4)$$

where $\Delta b'$ is compaction,
b_0' is the initial thickness of the compacting aquitard, and
Δh is the change in head of the compacting aquitard.

For a thick and (or) very low permeability aquitard, equation 4 represents the ultimate compaction that would occur after heads in the aquitard are equilibrated with the head decline in the adjacent, surrounding aquifer. The time constant (equation 2) can be used as a measure of the time for the ultimate compaction to occur in the aquitard following groundwater-level declines in the adjacent aquifers. The ultimate compaction may require decades or centuries. The residual compaction is the compaction yet to be realized as fluid pressures in the aquitard equilibrate with the initial groundwater-level decline in the surrounding aquifer. Ireland and others (1984) estimated time constants for aquitards at 15 sites in the San Joaquin Valley, California, that ranged from 5 to 1,350 years. Numerical modeling based on Terzaghi's theory has successfully simulated complex histories of compaction caused by known water-level fluctuations (Helm, 1978; Hanson, 1989; Sneed and Galloway, 2000). This time-delay component of compaction and accompanying subsidence, and its dependence on the aquitard thickness, makes comparison with current groundwater levels complicated in the Albuquerque Basin because of the relatively short study period and spatially variable thickness of clay-rich stratigraphic units. The description of subsidence in the Albuquerque Basin for this study is limited by the time period over which data have been collected and the extent of knowledge of the subsurface geology; however, the effective study period was extended by inclusion of previous land-surface elevation studies (Heywood and others, 2002) and long-term data records of subsidence, such as the Albuquerque extensometer.

The concepts reviewed in this section collectively form the aquitard-drainage model, which provides the theoretical basis of many successful subsidence studies related to the production of groundwater, oil, and gas. For a review of the history of the aquitard-drainage model, see Holzer (1984), for a more complete description of aquifer-system compaction, see Poland (1984), and for a review and selected case studies of land subsidence caused by aquifer-system compaction in the United States, see Galloway and others (1999).

Land Subsidence and Recovery

The measurement of land subsidence and recovery was completed using a variety of methods with different spatial and temporal coverages and compared to data from previous studies. Previous studies in the Albuquerque Basin have shown spatially heterogeneous aquifer-system compaction before 2005 (C.E. Heywood, U.S. Geological Survey, written commun., 1995; Heywood and others, 2002; Wilke, 2007). A Land-Subsidence Survey (LSS) network of 41 monuments was established by the USGS in 1993-94 (Wilke, 2007) (fig. 1). This LSS network was measured using network-based differential GPS techniques in 1994-95 and 2005 (Wilke, 2007). After a network correction to the 1994-95 data, a comparison of survey data from these studies shows vertical changes at these survey monuments; positive (+) values indicate a relative uplift whereas negative (-) values indicate a relative subsidence of the land surface. The difference in survey network values between surveys conducted in 1994-95 and 2005 ranges from +0.0275 m to -0.0363 m (Heywood and others, 2002; Wilke, 2007).

Extensometer

The Albuquerque borehole extensometer (USGS identification number 350836106395405) was installed in 1994 and is located within the Albuquerque Basin, east of the Rio Grande within the Rio Grande Valley (fig. 1) (Heywood, 1998). The Albuquerque extensometer measures vertical displacement of the sediments between 5 and 315 m below land surface relative to a given starting value. Vertical displacement is recorded at the Albuquerque extensometer using three methods: (1) continuous analog, (2) 30-minute interval digital, and (3) manual interval dial-gage readings. Continuous analog data are recorded using a Stevens Type F Chart Recorder (Stevens Recorder), which draws a line with a pen over time on scaled graph paper. Thirty-minute interval digital data are measured using a linear potentiometer and are scaled to convert millivolts output to vertical displacement distance. Dial-gage readings occur at each quarterly site visit; at which time, the Stevens Recorder graph paper is collected and replaced, and the digital data are downloaded. The redundancy of these three methods allows for backup if one or two of the methods are malfunctioning.

Analog data collection with the Stevens Recorder began on December 24, 1994, and the initial dial-gage reading at that time was 8.948 millimeters (mm). An aquifer test was conducted in the first months after analog data collection began, which showed the influence of groundwater pumpage on the vertical displacement measured at the Albuquerque extensometer. During pumping, the extensometer measured compaction; after the pumping stopped and groundwater levels recovered, the vertical displacement recovered to prepumping conditions (Prince and Leake, 1997).

Extensometer data used in this study start on April 6, 1995, the first time the Stevens Recorder paper was changed after the pump test was conducted. The dial-gage reading on April 6, 1995, was 11.069 mm. Extensometer analog and digital data were scaled and normalized to the dial-gage reading on this date. All measured deformation values are relative to this initial value, and increasing values indicate relative compaction. Vertical displacement data from April 6, 1995, to April 18, 2013, were analyzed for this report. Data from the Stevens Recorder were used until December 31, 2007, at which time the battery in the recorder began to fail. Data from the digital data collection were used from January 1, 2008, to April 18, 2013. These data were made to match the manual dial-gage readings when available, which occurred approximately quarterly, and converted to centimeters to relate to other vertical displacement values measured using other techniques. Data used for the analysis in this report can be found in the USGS National Water Information System (NWIS; https://doi.org/10.5066/F7P55KJN).

Aquifer-System Compaction Results

The vertical displacement measured by the Albuquerque extensometer shows seasonal variability of subsurface compaction over the time series of available data (fig. 2). Compaction values are seasonally low in the winter and high in the summer. This correlates well with seasonal pumping patterns in the Albuquerque Basin; more pumping occurs in the summer because of residential outdoor water use than in the winter (Powell and McKean, 2014; Beman and Bryant, 2016).

In order to quantitatively assess trends in extensometer data, annual minimum and maximum vertical displacement values, along with the date at which they were recorded, were identified for the period of record (table 1). The difference between annual minimum and maximum values is similar for each year (average difference between maximum annual and minimum annual vertical displacement is 4.22 mm, with a standard deviation of 0.9 mm).

Extensometer data show three trends over time: (1) a period of increasing compaction (about 1995–2003), (2) a period of stability (about 2004–7), and (3) a period of recovery (about 2008–13). Using the annual minimum vertical displacement values (table 1), correlation of these values over time was calculated to measure trends. The initial compaction period (about 1995–2003) showed high correlation between vertical displacement and time (Pearson's correlation coefficient [R^2; Helsel and Hirsch, 2002] value of 0.97, number of values [n] equals 8, and calculated probability [p] less than 0.05), and the rate of compaction was approximately 0.50 mm per year. The following period (about 2004–7) showed insignificant correlation between vertical displacement and time (R^2 value of 0.048, n equals 4, and p greater than 0.1). The following recovery period (about 2008–13) showed high correlation between vertical displacement and time (R^2 value of 0.86, n equals 6, and p less than 0.05), and the rate of recovery was approximately 0.35 centimeter per year (cm/yr).

These three trends show an overall change in aquifer-system response over time. The period of stability predates the SJCDWP and may show the effectiveness of actively managing groundwater withdrawals in conjunction with water conservation efforts by the ABCWUA. The period

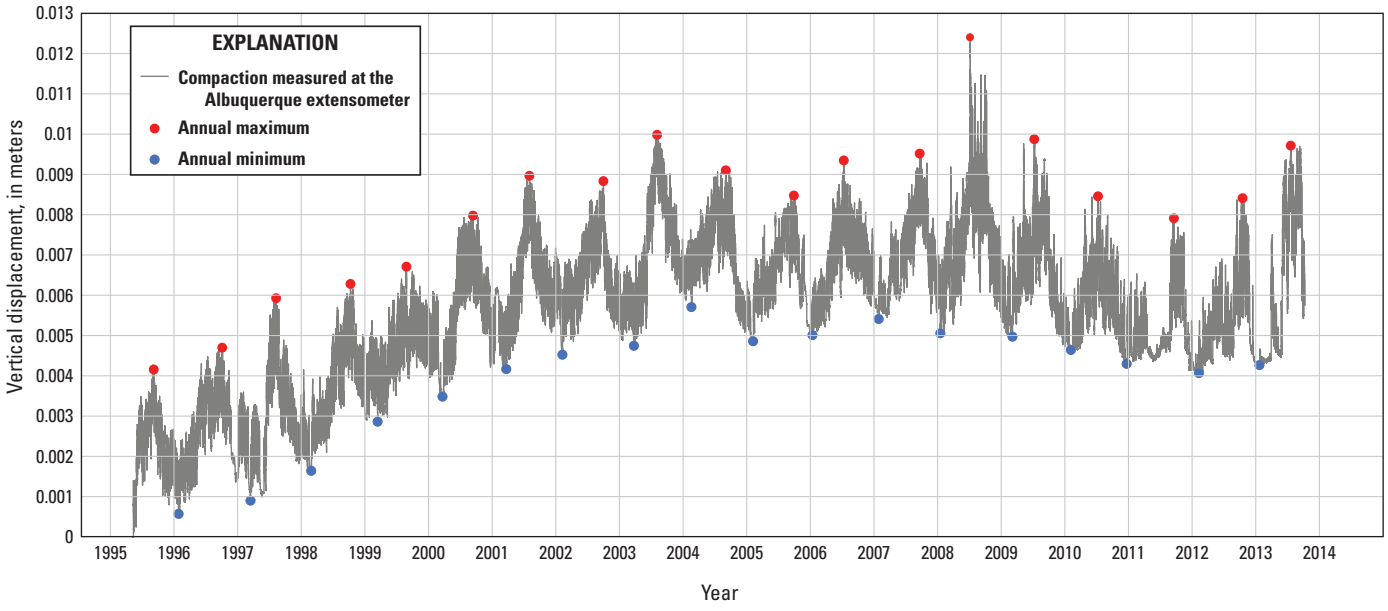

Figure 2. Time series of vertical displacement at the Albuquerque extensometer, April 6, 1995– April 18, 2013.

Table 1. Annual minimum and maximum vertical displacement values from April 6, 1995, to April 18, 2013.

[Dates in month, day, year; Annual minimums and maximums are in millimeters; Seasonal change is annual maximum minus annual minimum]

Date of annual minimum vertical displacement	Annual minimum vertical displacement	Date of annual maximum vertical displacement	Annual maximum vertical displacement	Seasonal change of vertical displacement
12/26/1995	0.6	7/30/1995	4.2	3.6
2/13/1997	0.9	9/3/1996	4.6	3.7
1/27/1998	1.6	7/10/1997	5.8	4.2
2/15/1999	2.8	9/11/1998	6.1	3.3
2/22/2000	3.4	7/31/1999	6.6	3.2
2/26/2001	4.1	8/18/2000	7.8	3.7
1/14/2002	4.4	7/9/2001	8.8	4.4
3/3/2003	4.6	9/8/2002	8.6	4.0
1/29/2004	5.6	7/14/2003	9.8	4.2
1/18/2005	4.7	8/13/2004	8.9	4.2
12/25/2005	4.9	9/10/2005	8.3	3.4
1/12/2007	5.3	6/25/2006	9.1	3.8
1/2/2008	4.9	9/5/2007	9.3	4.4
2/14/2009	4.9	6/21/2008	12.1	7.2
1/22/2010	4.5	6/26/2009	9.6	5.1
12/10/2010	4.2	6/28/2010	8.3	4.1
1/31/2012	4.0	9/9/2011	7.7	3.7
1/12/2013	2.8	9/5/2012	7.7	4.9

of recovery corresponds to the 2008 start of the SJCDWP providing surface-water supply for the city of Albuquerque. These data suggest the reduction in groundwater pumpage not only allowed for groundwater level recovery (Powell and McKean, 2014; Beman and Bryant, 2016) but also elastic recovery (expansion) of the aquifer system underlying the Albuquerque Basin.

Aquifer-System Compaction and Depth-to-Groundwater Level Analysis

The correlation of the Albuquerque extensometer aquifer-system compaction data and depth-to-groundwater level data (measured at Montaño 6 monitoring well USGS identification number 350836106395401, located approximately 1 km from the extensometer and screened from 297 to 298 m below land surface) were analyzed for synoptic (fig. 3) and daily (fig. 4) depth-to-groundwater values. These analyses were limited by the timing of groundwater data collection at Montaño 6. Synoptic manual depth-to-groundwater measurements are available from 1997 through 2013, whereas daily depth-to-groundwater measurements are available from 2008 to 2012 (USGS NWIS; https://doi.org/10.5066/F7P55KJN).

Depth to groundwater is used as a measure of stress in the aquifer system, and aquifer-system compaction is used as a measure of displacement. The skeletal specific storage, S_k (equation 3), was calculated for groups of data as the inverse slope of the linear regression of depth to groundwater and compaction values by

$$S_k = (\gamma_w \alpha) b \tag{5}$$

where γ_w is the specific weight of water,
α is the aquifer-system skeletal (matrix) compressibility, and
b is the thickness of the aquifer system.

S was computed as the sum of S_k and the storage coefficient of water (S_w) where

$$S_w = (\gamma_w n \beta_w) b = 4.1 \times 10^{-4} \tag{6}$$

where b is equal to 315 m,
β_w is equal to 4.4×10^{-10} kg·m^{-1}·s^{-2},
γ_w is equal to 9,800 kg·m^{-2}·s^{-2}, and
n is equal to 0.3.

In order to compare subdaily extensometer aquifer-system compaction data to daily and synoptic depth-to-groundwater data, extensometer data were summarized to mean daily values and compared to depth-to-groundwater-level data collected on the same day. Data were divided into four season-based groups before and after the SJCDWP: (1) winter 1997–2008, (2) summer 1997–2008, (3) winter 2008–13, and (4) summer 2008–13. The break in the time series at 2008 allows for investigation of data before and after the SJCDWP began.

The correlations between depth to groundwater and compaction for seasonal groups before the SJCDWP began (1997-2008) were less significant (p less than 0.10) than after the SJDWP began (p less than 0.0001) (fig. 3). The correlation between depth to groundwater and compaction for winter 1997–2008 is lower ($R^2 = 0.04$) than summer 1997–2008 ($R^2 = 0.5$) because of low groundwater pumping in the winter months relative to summer months. Increased correlation between depth to groundwater and aquifer-system compaction for the winter 2008–13 ($R^2 = 0.8$) and summer 2008–13 ($R^2 = 0.8$), relative to before the SJCDWP, indicates effects of aquifer recovery throughout the year because of less overall groundwater pumping.

Calculated estimates for skeletal storage (S_k) and storage (S) are shown in table 2 with estimates computed from a pumping test at the Montaño 6 site in 1997 (Heywood, 1998). These data show a substantially greater S_k (arising from greater α) in the winter prior to the SJCDWP relative to all other values. There is a small decrease in S_k between summer before and after SJCDWP and a substantial decrease between winter before and after SJCDWP.

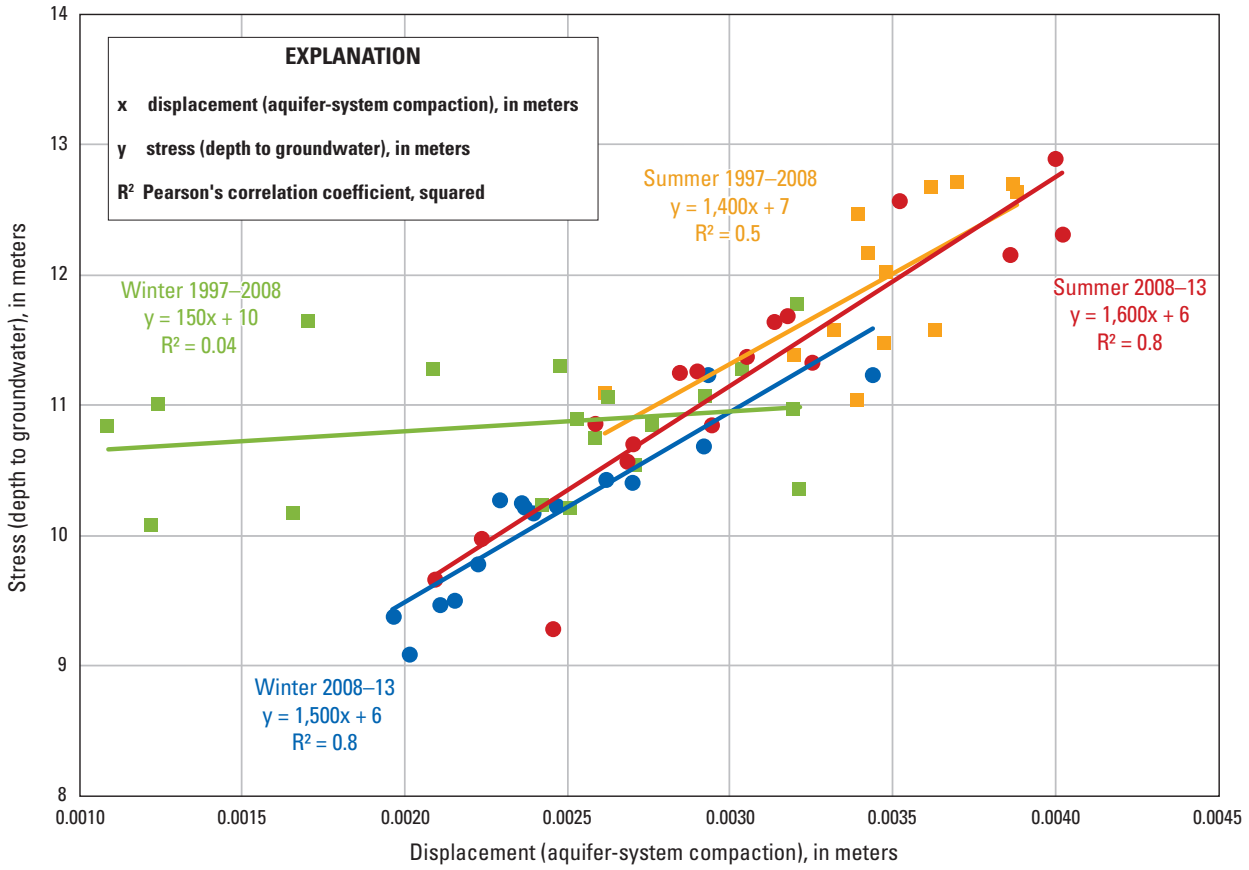

Figure 3. Synoptic depth-to-groundwater level measurements relative to the daily mean aquifer-system compaction measurements on the same day from 1997 to 2013.

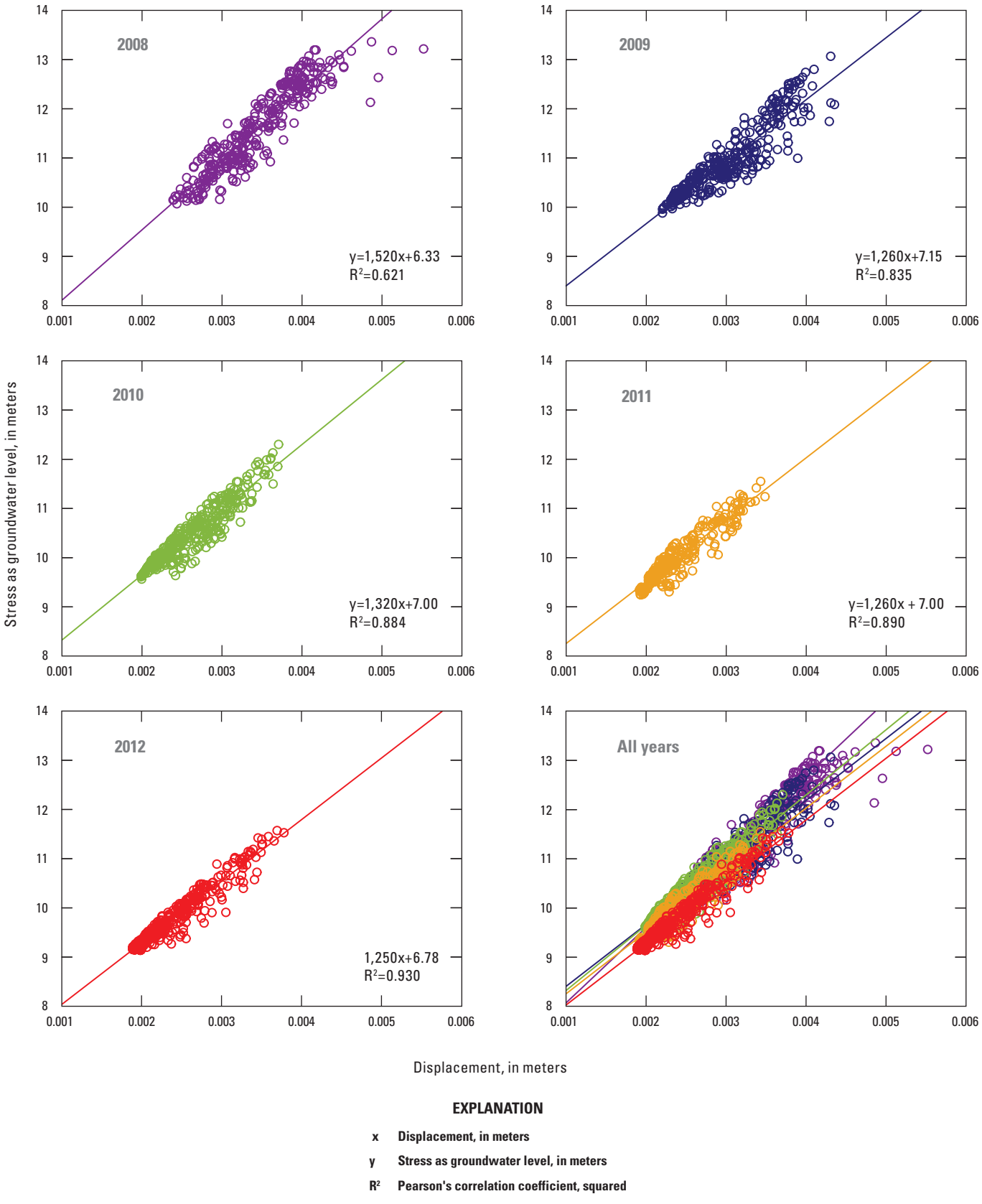

Figure 4. Daily values of displacement (aquifer-system compaction) and stress (depth-to-groundwater level) and linear regressions for each year, 2008–12.

Table 2. Aquifer-system skeletal storage (S_k) and storage (S) (the sum of S_k and the storage coefficient of water S_w) for different time periods.

[*, data from Heywood, 1998; NA, not applicable]

Data frequency	Time period	S_k	S ($S_k + S_w$)
NA	1997*	1.5×10^{-3}	1.9×10^{-3}
Synoptic	Winter 1997–2008	6.7×10^{-3}	7.1×10^{-3}
	Summer 1997–2008	7.1×10^{-4}	1.1×10^{-3}
	Winter 2008–13	6.7×10^{-4}	1.1×10^{-3}
	Summer 2008–13	6.3×10^{-4}	1.0×10^{-3}
	Winter 2009–13	6.7×10^{-4}	1.1×10^{-3}
	Summer 2009–13	6.3×10^{-4}	1.0×10^{-3}
Daily	2008	6.7×10^{-4}	1.1×10^{-3}
	2009	7.7×10^{-4}	1.2×10^{-3}
	2010	7.7×10^{-4}	1.2×10^{-3}
	2011	7.7×10^{-4}	1.2×10^{-3}
	2012	7.7×10^{-4}	1.2×10^{-3}

Automated daily mean depth-to-groundwater data were collected at the Montaño 6 well from 2008 through 2012. These daily mean depth-to-groundwater data were plotted against mean daily compaction data measured at the extensometer, grouped by each year (fig. 4). Linear regressions of these data were used to compute estimates of aquifer-system S_k and S coefficients for each year, same as the synoptic seasonal data. The slope (and therefore S_k, which is equal to the inverse slope of the regression) is fairly consistent, with S_k values equal to 1.43×10^{-3}, 1.27×10^{-3}, 1.33×10^{-3}, 1.27×10^{-3}, 1.27×10^{-3} (2008–12, respectively). The magnitude of daily stress and displacement values overall decrease from 2008 to 2012. This decrease reflects an overall reduction in elastic deformation for the aquifer system.

Synoptic and daily data show a direct relation over time, generally with increasing depth-to-water values corresponding to increasing compaction and allowing for the conclusion that changing groundwater levels in the Albuquerque Basin lead to changes in aquifer-system deformation (compaction and expansion) and resulting in changes in land-surface elevation. The extent to which this relation can be spatially extrapolated has not been determined because of the single extensometer in the basin; however, further analysis of aquifer characteristics may help to explain this relation.

Global Positioning System Surveys

The GPS surveys utilize earth orbiting satellites to precisely triangulate horizontal position and elevation. Accurate elevation measurement with GPS is substantially more difficult than horizontal location measurement; survey-grade GPS equipment and specific methods are required to achieve measurements with errors within the range of 2 cm, useful for land-surface subsidence studies. The repeated measurement of the elevation at the same location using these methods provides information on the change in elevation at that location over time.

Land-Subsidence Survey Network

The LSS network of 41 monuments (fig. 1) was developed in 1993–94 (Wilke, 2007). Monuments include caps in existing infrastructure (in concrete pads on or near roadways), as well as metal rods driven into the ground. Ellipsoid heights (relative to the GPS satellite reference frame) measured at monuments are used to compute land-surface elevations at each monument location based on a geoid model. Comparison of the elevations provides information on changes in elevation at the same point over time.

Land-Subsidence Survey Methods

The GPS network-based differential survey methods were used in 1994–95 and 2005. While spirit leveling survey techniques continue to be the most accurate method for determining vertical elevation difference, advances in GPS technology allow for use of more efficient survey techniques with minimal sacrifice of accuracy. Two GPS survey techniques, followed by postprocessing to convert measured ellipsoid heights to elevation, were used in this study: (1) network-based differential, and (2) rapid-static occupation. Network-based differential surveying can be accurate within 1 cm, but considerable postprocessing is required and the technique can be prone to errors such as tilt bias (Wilke, 2007). The National Geodetic Survey's Online Positioning User Service (OPUS) postprocessing algorithm can be accurate within 2 cm but is significantly simpler because of the automatic postprocessing that is available online (https://www.ngs.noaa.gov/OPUS/). Network-based differential surveys also require several points to be fixed for reference, which removes these points from spatial coverage of the network in terms of measuring change in elevation. Rapid-static occupation processed with OPUS was used to conduct the GPS survey and process the data, respectively, in the summer of 2014.

The 1994–95 survey was completed by the USGS after the installation of the LSS monuments using network-based differential survey techniques (Heywood, 1998). The 2005 survey was completed by the city of Albuquerque using network-based differential survey techniques (Wilke, 2007). While generating the elevation results for the differential network for the monuments in 2005, a network-wide tilt was discovered in the 1994–95 survey data. A correction was applied to these data to adjust for the tilt bias in the original data. The ellipsoid elevation (height) results from each of these LSS network surveys are presented in table 3.

Table 3. Monument ellipsoid heights from the 1994–95, 2005, and 2014 surveys.

[ND, no data; *, monument was disturbed; **bold**, change in ellipsoid height is greater than the maximum combined error of measurements; *italics*, change in ellipsoid height is less than maximum combined error of measurements]

Monument identification number	Latitude	Longitude	1994–95 Ellipsoid height[1] (meters)	1994–95 Ellipsoid height error[1] (centimeters)	2005 Ellipsoid height[1] (meters)	2005 Ellipsoid height error[1] (centimeters)	2014 Ellipsoid height (meters)	2014 Ellipsoid height error (centimeters)	Root mean square of 1994–95 and 2005 survey error values (centimeters)	Root mean square of 2005 and 2014 survey error values (centimeters)	Change in Ellipsoid height (2005 minus 1994–95) (centimeters)	Change in Ellipsoid height (2014 minus 2005) (centimeters)
11_H23	35.11020	-106.487	1,874.7342	0.65	1,874.7342	0.00	ND	ND	0.65	ND	0 (fixed)	ND
2_U10	34.94994	-106.716	1,518.9173	0.76	1,518.9385	1.11	ND	ND	1.35	ND	**2.12**	ND
A_425	35.02744	-106.965	1,615.2131	0.89	1,615.2131	0.00	1,615.310	0.20	0.89	0.20	Fixed	**9.69**
A_438	35.11052	-106.642	1,495.1872	0.63	1,495.1792	0.78	1,495.194	2.30	1.00	2.43	*-0.80*	*1.48*
C_438	35.12852	-106.635	1,496.5159	0.98	ND	ND	ND	ND	ND	ND	ND	ND
CAL_STA_A	35.15313	-106.728	1,603.0263	0.61	1,603.019	0.69	1,603.025	1.10	0.92	1.30	*-0.73*	*0.60*
COYOTE	34.98804	-106.509	1,715.5708	0.86	1,715.5741	1.01	1,715.555	3.80	1.32	3.93	*0.33*	*-1.91*
E_438	35.17942	-106.616	1,502.6801	0.68	1,502.6721	0.86	ND	ND	1.10	ND	*-0.80*	ND
EAGLEAIR	35.14512	-106.786	1,746.5986	ND	1,746.5929	0.66	1,746.588	0.50	ND	0.83	-0.57	*-0.49*
FLP_9_60	35.19805	-106.644	1,505.9912	0.83	1,505.9875	0.94	1,505.969	0.80	1.25	1.23	*-0.37*	**-1.85**
G_438	35.20857	-106.598	1,515.1510	1.17	1,515.2167	1.00	ND	ND	1.54	ND	**6.57**	ND
GLORIA	35.07210	-106.483	1,866.1450	0.75	1,866.1725	0.62	1,866.139	5.00	0.97	5.04	**2.75**	*-3.35*
LSS_101	35.20144	-106.541	1,675.5201	0.91	1,675.5081	0.92	1,675.476	0.90	1.29	1.29	*-1.20*	**-3.21**
LSS_102	35.20420	-106.577	1,567.4156	0.85	1,567.410	1.04	ND	ND	1.34	ND	*-0.53*	ND
LSS_103	35.20570	-106.703	1,592.6544	0.69	1,592.6415	0.87	1,592.632	0.40	1.11	0.96	*-1.29*	*-0.95*
LSS_104	35.24144	-106.745	1,698.7971	0.63	1,698.7866	1.16	1,698.811	3.00	1.32	3.22	*-1.05*	*2.44*
LSS_105	35.24434	-106.856	1,850.2557	0.54	1,850.2557	0.00	1,850.239	0.80	0.54	0.80	0 (fixed)	**-1.67**
LSS_106	35.18920	-106.476	2,026.5592	0.69	2,026.5484	1.07	2,026.503	1.50	1.27	1.84	*-1.08*	**-4.54**
LSS_201	35.14152	-106.498	1,798.9174	0.78	1,798.9006	0.77	1,798.868	2.90	1.09	3.00	**-1.68**	*-3.26*
LSS_202	35.13015	-106.521	1,707.9970	0.86	1,707.9807	0.75	ND	ND	1.14	ND	**-1.63**	ND
LSS_203	35.13222	-106.549	1,640.4116	0.88	1,640.3908	0.89	1,640.368	0.60	1.25	1.07	**-2.08**	**-2.28**
LSS_204	35.13094	-106.573	1,590.8574	0.91	1,590.830	0.95	1,590.810	ND	0.65	ND	**-2.72**	*-2.02*
LSS_205	35.13442	-106.597	1,547.1078	0.86	ND	ND	1,546.990	ND	1.35	ND	ND	ND
LSS_206	35.14014	-106.651	1,495.5819	0.76	1,495.5928	1.52	1,495.611	0.20	0.89	0.20	*1.09*	*1.82*

Table 3. Monument ellipsoid heights from the 1994–95, 2005, and 2014 surveys.—Continued

[ND, no data; *, monument was disturbed; **bold**, change in ellipsoid height is greater than the maximum combined error of measurements; *italics*, change in ellipsoid height is less than maximum combined error of measurements]

Monument identification number	Latitude	Longitude	1994–95 Ellipsoid height[1] (meters)	1994–95 Ellipsoid height error[1] (centimeters)	2005 Ellipsoid height[1] (meters)	2005 Ellipsoid height error[1] (centimeters)	2014 Ellipsoid height (meters)	2014 Ellipsoid height error (centimeters)	Root mean square of 1994–95 and 2005 survey error values (centimeters)	Root mean square of 2005 and 2014 survey error values (centimeters)	Change in Ellipsoid height (2005 minus 1994–95) (centimeters)	Change in Ellipsoid height (2014 minus 2005) (centimeters)
LSS_301	35.07482	-106.508	1,686.4449	0.87	1,686.4412	0.64	1,686.424	2.30	1.00	2.43	*-0.37*	*-1.72*
LSS_302	35.06751	-106.539	1,638.6790	0.86	1,638.6701	0.96	1,638.660	ND	ND	ND	*-0.89*	*-1.01*
LSS_303	35.06203	-106.613	1,586.6897	0.83	1,586.7072	1.10	1,586.689	1.10	0.92	1.30	*1.75*	*-1.82*
LSS_304	35.07167	-106.691	1,485.5442	0.7	1,485.5383	1.29	1,485.587	3.80	1.32	3.93	*-0.59*	**4.87**
LSS_401	34.94720	-106.569	1,584.2127	0.88	1,584.2127	0.00	1,584.193	ND	1.10	ND	0 (fixed)	*-1.97*
LSS_402	34.95136	-106.673	1,482.6985	0.78	ND	ND	ND	0.50	ND	0.83	ND	ND
LSS_501	35.24718	-106.670	1,616.6651	0.81	ND	ND	ND	0.80	1.25	1.23	ND	ND
LSS_502	35.27280	-106.663	1,657.6311	0.94	1,657.655	1.13	ND	ND	1.54	ND	**2.39**	ND
LSS_503	35.27342	-106.733	1,753.5898	0.75	1,753.5966	1.48	1,753.551	5.00	0.97	5.04	*0.68*	**-4.56**
LSS_504	35.26243	-106.774	1,738.6265	0.68	1,738.5945	1.19	1,738.592	0.90	1.29	1.29	**-3.20**	*-0.25*
NEC	35.23062	-106.992	1,766.3905	0.66	1,766.366	0.90	ND	ND	1.34	ND	**-2.45**	ND
NM_BER_400	35.20226	-106.504	1,836.4012	0.83	1,836.4015	1.31	1,836.336	0.40	1.11	0.96	*0.03*	**-6.55**
Q_424	35.07064	-106.778	1,693.9535	0.55	1,693.9481	0.83	1,693.94	3.00	1.32	3.22	*-0.54*	*-0.81*
SAT_TRI_110	34.94545	-106.460	1,810.3095	0.84	1,810.310	0.00	1,810.294	0.80	0.54	0.80	0 (fixed)	**-1.55**
SQAW	35.13061	-107.014	ND	ND	1,733.4576*	1.14	ND	1.50	1.27	1.84	ND	ND
U_424	35.05059	-106.863	ND	ND	1,770.3917	1.01	1,770.424	2.90	1.09	3.00	ND	**3.23**
UNION	35.18642	-106.741	1,662.6432	0.61	1,662.6409	0.72	1,662.618	ND	1.14	ND	*-0.23*	**-2.29**

[1]Data from report by Wilke, 2007.

The amount of time was not recorded for collection of the ellipsoid height data during the 1994–95 and 2005 surveys. Extensometer data suggest substantial seasonal variation (relative to annual variation) in elevation because of seasonal pumping variability and deformation of the aquifer (fig. 2). This seasonal elevation change was accounted for in the 2014 survey by conducting the survey over a 4-week period in June and July of 2014. During this time period, the range between vertical displacement values measured at the extensometer (the difference between the first and third quartile values) was 0.04 cm. Seasonal variability in the collection of benchmark elevation data as well as annual variability were minimized by shortening the time of data collection in 2014; however, seasonal variability may be an issue in comparison with other surveys because the period of time is unknown over which data were collected. Without information about the duration or timing of these earlier surveys, it is not known if they are winter (minimum drawdown), summer (maximum drawdown), or a mixture of both. If seasonal variability is higher than annual variability, this could result in misleading changes in elevation values between surveys.

Land-Subsidence Survey Network Results

The ellipsoid heights were compared from each of the three surveys to determine height changes of each monument between 1994–95 and 2014. The direction and magnitude of elevation change are shown in table 3. Negative values indicate that the elevation decreased between surveys, whereas positive values indicate that the elevation increased between surveys. The direction of elevation change calculations for each monument was mapped to visualize the spatial distribution of land-surface elevation trends in the study area (fig. 5).

The urban setting of the LSS led to a number of the original monuments being moved or destroyed as a result of construction or other disruptions over the timespan of the project (1993–2014), resulting in no data collection. No usable data were collected at five monuments for any of the surveys (monuments IDs: C_438, LSS_205, LSS_402, LSS_501, SQAW). Eight monuments were destroyed, disturbed, or otherwise inaccessible for at least one of the surveys (11_H23, 2_U10, E_438, G_438, LSS_102, LSS_202, LSS_502, and NEC), resulting in insufficient data to calculate the elevation change at these locations. There are 26 monuments with ellipsoid height change data from both early and late (from 1994–95 to 2005 and 2005 to 2014, respectively) time periods. Of these 26 monuments with change in ellipsoid heights, only some have a change greater than the cumulative error (uncertainty) reported for the individual monument survey data; there are 10 from 1994–95 to 2005 and 12 from 2005 to 2014 (table 3).

Thirteen monuments (EAGLEAIR, FLP_9_60, LSS-101, LSS_103, LSS_106, LSS_201, LSS_203, LSS_204, LSS_301, LSS_ 302, LSS_504, Q_424, and UNION) show a decrease in ellipsoid height for both early and late time periods. Four monuments (A_438, CAL_STA_A, LSS_304, and LSS_104) show a decrease in ellipsoid height during the early time period and an increase in elevation during the later time period. Five monuments (COYOTE, GLORIA, LSS_303, LSS_503, and NM_BER_400) show an increase in elevation during the early time period and a decrease in ellipsoid height during the later time period. One monument (LSS_206) shows an increase in ellipsoid height for both early and late time periods. Two monuments (A_425 and U_424) show no values for difference in ellipsoid height during the early time period (A_425 because it was a fixed reference for the network and U_424 because no data were collected in the earliest survey) and an increase in ellipsoid height during the later time period. Three monuments (LSS_105, LSS_401, and SAT_TRI_110) show no values for difference during the early time period (because they were fixed reference for the network) and a decrease in ellipsoid height during the later time period. Three monuments (LSS_502, 2_U10, and G_438) show an increase in ellipsoid height during the early time period and were destroyed during the later time period, resulting in no data. Three monuments (LSS-102, LSS-202, and NEC) show a decrease in ellipsoid height during the early time period but were destroyed or inaccessable during the later time period, resulting in no data. One monument (11_H23) shows no values for difference in elevation during the early time period because it was fixed reference for the network and was destroyed during the later time period, resulting in no data.

These point measurements of elevation change between GPS surveys do not show a clear spatial trend of where and when land-surface elevation was changing. This could be a result of a strong seasonally affected elevation change because pumpage from groundwater was larger than annual or overall trend. The seasonal timing of the differential network surveys (1994–95 and 2005) is not known, but the 2014 survey was conducted in June and July 2014 when seasonal groundwater pumpage was high. If the other two surveys were conducted in the winter, when seasonal groundwater pumpage was low, this could bias the later time period data to show a decrease in elevation because of the seasonal groundwater pumpage variability. The lack of spatial pattern of elevation trend over the study may suggest the seasonal timing of the surveys was not consistent, or may reflect monument instability, heterogeneous geology, water-level declines, and (or) surveying errors.

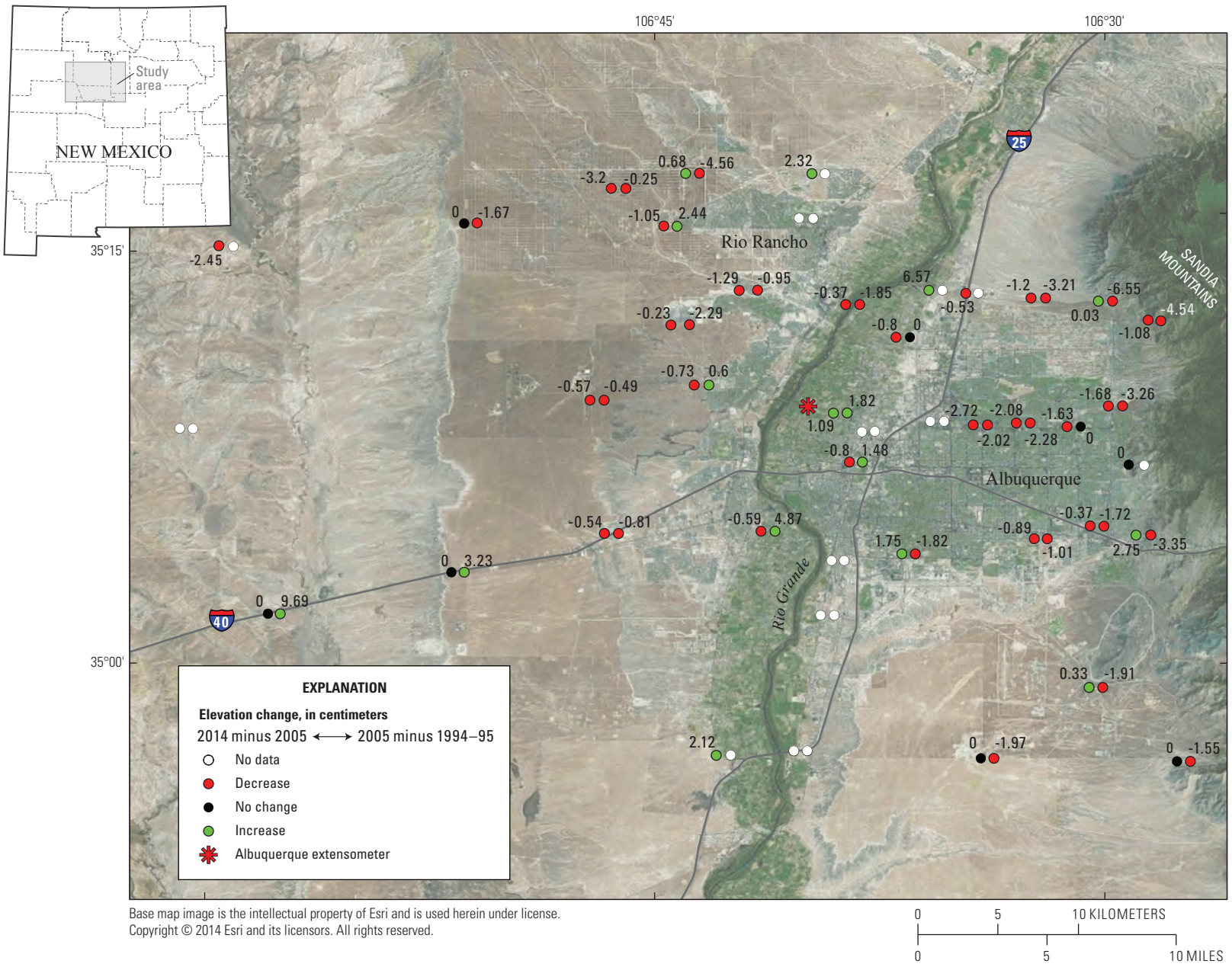

Figure 5. Elevation change between Global Positioning System (GPS) surveys at land-surface subsidence network monuments.

Interferometric Synthetic Aperture Radar

Interferometric Synthetic Aperture Radar (InSAR) is an effective way to measure vertical changes of land surface. InSAR is a satellite-based remote sensing technique that can detect centimeter-level, ground-surface displacement over thousands of square kilometers with a 30×30-m spatial resolution. This technique has been used to investigate deformation resulting from earthquakes (Massonnet and others, 1993), volcanoes (Massonnet and others, 1995), and land subsidence attributed to subsurface fluid extraction (Massonnet and others, 1997; Fielding and others, 1998; Galloway and others, 1998; Amelung and others, 1999; Hoffmann and others, 2001; Sneed and Brandt, 2007; Sneed and others, 2013, 2014). Synthetic Aperture Radar (SAR) imagery is produced by reflecting sinusoidal radar signals off a target area and measuring the two-way traveltime back to the satellite. The SAR interferometry technique uses two SAR images of the same area acquired at different times and interferes (differences) them, resulting in maps called interferograms that show line-of-sight ground-surface displacement (range change) between the acquisition dates of the two images. The generation of an interferogram produces the components amplitude and phase. The amplitude component is the measure of the radar signal intensity returned to the satellite and shows buildings, roads, mountains, and other reflective features. The phase component is the portion of the sine wavelength reflected back to the satellite and is proportional to the line-of-sight distance to the ground. If the ground has moved away from (subsidence) or towards (uplift) the satellite between the times of the two acquisitions, a slightly different portion of the wavelength is reflected back to the satellite, resulting in a measurable phase shift. For this study, a map of the spatial distribution of these phase shifts (interferogram) is depicted with a repeating color scale (rainbow: red, orange, yellow, green, blue, indigo, and violet) that shows relative range change, where one complete color cycle (fringe) represents 28.3 mm of range change (one-half the wavelength of the C-band radar on the SAR satellite used in this study). Phase shift values repeat for each full wavelength (from 0 to 2 pi), so when a phase shift greater than one-half the radar wavelength occurs between two points, the data values wrap back to zero. For detailed analysis, the phase-shift data must be unwrapped in order to determine ground displacement values. The direction of change—subsidence or uplift—is indicated by the color progression of the fringe toward the center of a deforming feature. Interferograms in this report were interpreted such that green depicts land-surface stability, with the progression of colors on the color scale leading from green indicating the direction of the deformation: green→blue→indigo→violet→red indicates relative uplift, and green→yellow→orange→red→violet indicates relative subsidence.

The high spatial resolution of InSAR imagery can be used to infer the locations of buried faults not readily evident on the surface (Galloway and others, 1999; Sneed and Brandt, 2007) that may act as barriers to groundwater flow and (or) separate hydrostratigraphic units with differing hydromechanical properties. In order to infer the locations of groundwater-flow barriers using InSAR, generally a hydraulic stress (for example, groundwater pumping or recharge) must occur in compaction-susceptible water-bearing deposits in the vicinity of a fault or groundwater barrier. The greater the deformation rate, the more easily the lineament can be identified as a steep spatial gradient of displacements on the interferogram, and thus facilitate a more robust identification of groundwater-flow barriers in the InSAR imagery because the differential uplift or subsidence on either side of the lineament is more pronounced. The identification of these features is important because the tensional stresses that develop near the region of differential land-surface displacement can promote the formation of earth fissures and (or) motion on surface faults (Holzer, 1984) and create hazards for infrastructure and land use. Earth fissures and (or) motion on surface faults associated with land subsidence caused by groundwater-level declines have been identified in many locations in the Southwest including Arizona, California, Nevada, Texas, and Utah, and in the Mimbres Basin in New Mexico (Holzer and Pampeyan, 1981; Holzer, 1984; Contaldo and Mueller, 1991a, 1991b; Haneberg and Friesen, 1995; Bell and Helm, 1998; Holzer and Galloway, 2005; Lund and others, 2005; Conway, 2016).

Interferometric Synthetic Aperture Radar Uncertainty

The InSAR signal quality is dependent on a combination of factors: satellite position, phase shifts caused by topography and atmospheric effects, ground cover, land-use practices, and timespan of the interferogram. Each of these sources of uncertainty is briefly described in this section in addition to the steps taken to reduce or eliminate them. More detailed descriptions of InSAR methodology and sources of uncertainty can be found in Sneed and others (2014).

Strict orbital control is required to precisely control the angle and position of the satellite radar. Successful application of the InSAR technique is contingent on measuring the same point (target) on the ground from approximately the same position in space for repeat passes of the satellite, such that the horizontal distance (perpendicular baseline) between each satellite pass is minimized. Perpendicular baselines generally greater than about 200 m produce excessive topographic effects (parallax) that can mask actual displacement. For this study, the relatively flat topography of the Albuquerque Basin allowed the inclusion of SAR image pairs with perpendicular baselines of as much as 300 m without adversely affecting the ability to interpret interferograms.

Phase shifts can also be caused by laterally variable atmospheric conditions such as clouds or fog because the nonuniform distribution of water vapor differentially slows the radar signal over an image (Zebker and others, 1997). Phase shifts can also be caused by variable atmospheric mass that

is associated with different elevations (stratified atmosphere). For this study, phase shifts caused by atmospheric artifacts were identified and removed using analysis further described in Sneed and others (2014).

The type and density of ground cover can affect interferogram quality. Densely forested areas are prone to poor signal quality because the radar wavelength cannot effectively penetrate thick vegetation and is either absorbed or reflected back to the satellite from varying depths within the canopy, resulting in an incoherent signal (shown as randomized colors on an interferogram). Sparsely vegetated areas and urban centers, however, generally have high signal quality because bare ground, roads, and buildings have high reflectivity and tend to be uniform during the range of InSAR timescales (repeat orbit period). Certain land use practices, such as farming, also cause incoherent signal return. The tilling and plowing of farm fields causes large and nonuniform ground-surface change that cannot be resolved with InSAR.

Signal quality also is adversely affected by larger interferogram time spans because there is more opportunity for nonuniform change to occur in urban and nonurban areas. Many of these error sources were minimized by examining several independent interferograms for the study area, which is primarily urban or sparsely vegetated and topographically flat.

Interferometric Synthetic Aperture Radar Data

For this study of the Albuquerque Basin, C-Band (56.6 mm wavelength) SAR data from the European Space Agency's Environmental Satellite (ENVISAT, https://directory.eoportal.org/web/eoportal/satellite-missions/e/envisat) were used to measure and map deformation. The satellite's radar is side-looking, and the satellite orbits the Earth at an altitude of about 800 km, with a 35-day repeat cycle. The angle between vertical and the look angle, or angle of incidence, of the radar beam is about 23 degrees, which means that vertical deformation is about 92 percent of the measured range change.

Ninety interferograms with timelines ranging from 35 to 1,750 days were developed for this study using 42 ENVISAT SAR scenes acquired from 2005 to 2010. A base map was used as a visual guide to identify potential topography-related errors and for georeferencing of the interferograms. Continuous GPS (CGPS) data from station P034 (UNAVCO, 2015) (fig. 1) were used to ground truth the SAR data (fig. 6). Interferograms used for time-series analyses were selected based on qualitative image quality and favorable comparison with CGPS data. For selected locations, deformation magnitudes in each interferogram were interpreted and rounded to the nearest half centimeter. Five back-to-back (sequential and continuous in time) interferograms between 2005 and 2010 were selected to construct a deformation time series at select locations in order to compare InSAR-measured deformation with available depth-to-groundwater records.

Additionally, deformation profiles were constructed using five back-to-back (continuous) interferograms along geologic profiles for two time periods: August 22, 2005–June 2, 2008, and July 7, 2008–June 7, 2010, which corresponded to time periods approximately before and after summer of 2008 when the ABCWUA reduced their groundwater pumpage volume (ABCWUA, 2009) and groundwater recovery began (Beman and Bryant, 2016).

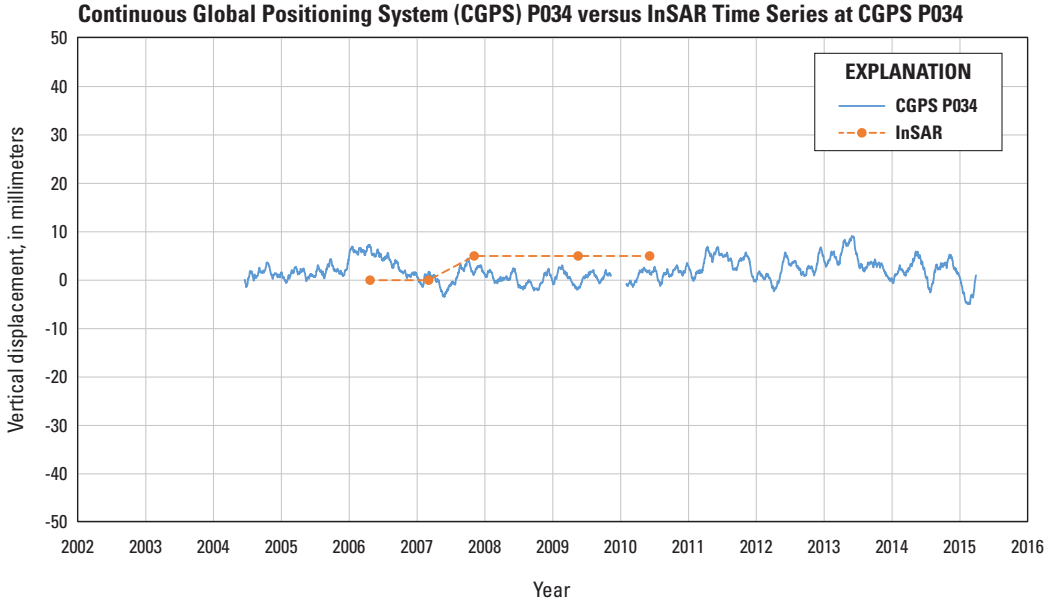

Figure 6. Vertical displacement measured by continuous Global Positioning System (CGPS) and Interferometric Synthetic Aperture Radar (InSAR) at site P034.

Interferometric Synthetic Aperture Radar Results

The InSAR results indicate spatially heterogeneous and seasonally dependent uplift and subsidence features within the Albuquerque Basin and surrounding area. Overall results do not show substantial subsidence in the Albuquerque Basin, but these data do allow for assessment of aquifer-system response to recovering groundwater levels. Selected composite and individual interferograms are presented, which provide an overview of overall deformation over the study period as well as seasonal and annual deformation before and after changes in groundwater pumping in the Albuquerque Basin because of the SJCDWP in 2008 (figs. 6 and 7).

Composite Interferogram

A composite interferogram, composed of five continuous interferograms between August 2005 and June 2010, shows deformation over the study area for the longest period possible during the study period given ENVISAT SAR data availability and quality (fig. 7).

The composite interferogram indicates a 20- to 28-mm uplift feature generally east of the Rio Grande encompassing nearly the entire Albuquerque Basin, where approximately 20 mm of uplift occurred within the southern reaches of the main feature near the Albuquerque International Airport. This composite interferogram shows spatially complex deformation patterns where approximately 1-2 km wide uplift features are adjacent to similarly sized subsidence features (for example, the 10-mm subsidence and 10-mm uplift features east of the town of Rio Rancho; fig 7). Composite InSAR imagery also indicates a maximum uplift of about 28 mm occurred in two approximately 1-km wide features about 10 km west of Interstate 25 and 8 and 11 km north of Interstate 40 during 2005 to 2010.

Annual and Seasonal Interferograms

Four interferograms were selected to show annual and seasonal land-surface-elevation change over the study period: (1) between March 20, 2006, and March 5, 2007 (fig. 8*A*); (2) between January 29, 2007, and February 18, 2008 (fig. 8*B*); (3) between November 5, 2007, and June 2, 2008 (fig. 8*C*); and (4) between July 7, 2008, and June 7, 2010 (fig. 8*D*). Three of these interferograms (figs. 8*A*, *B*, and *D*) span annual periods and one (fig. 8*C*) spans a 7-month period from fall to spring.

Three of the interferograms (figs. 8*A–C*) represent a time period of about 1 year or less and show most of the study area is stable (green) with smaller scale (approximately 3 km wide) subsidence features occurring near Rio Rancho (for example, figs. 8*A–C*) and near Interstate 40, west of the Rio Grande (for example, figs. 8*A* and 8*B*). Approximately 10 mm of uplift also occurred west of Rio Rancho between January 29, 2007, and February 18, 2008 (fig. 8*B*). The fourth interferogram (fig. 8*D*) represents a time period of approximately 2 years and indicates three areas approximately 3 km wide of about 20 mm of uplift within a broader (approximately 15 km by 35 km) uplift feature generally located west of Interstate 25 and north of Interstate 40.

Measurement of Land Deformation and Mapping of Structural Control

Faults that act as barriers to groundwater flow and (or) separate hydrostratigraphic units with contrasting hydromechanical properties are plausible in the Albuquerque Basin because it is extensively faulted (approximate and concealed faults from Connell, 2006). In alluvial basins, there can be a juxtaposition of consolidated rocks against partly consolidated or unconsolidated water-bearing deposits or preferential flow paths in the partly consolidated or unconsolidated water-bearing deposits (Galloway and others, 1999). This juxtaposition and displacement, in conjunction with cementation, compaction, and deformation of water-bearing deposits adjacent to faults, can create low-permeability zones that can act as barriers to groundwater flow and can separate hydrostratigraphic units with contrasting hydromechanical properties. Groundwater-flow barriers are not readily identified in the Albuquerque Basin at a coarse scale (Powell and McKean, 2014), and the influence of faults on groundwater flow at a finer scale is unknown.

The InSAR imagery processed for this report indicates several lineaments that truncate land-surface deformation features (white lines in figs. 7 and 8). These lineaments generally coincide with existing fault locations or are close to and nearly parallel to previously mapped faults, which suggests some lineaments are unmapped extensions of previously mapped faults that act as barriers to groundwater flow and (or) separate hydrostratigraphic units with contrasting hydromechanical properties. Regions in the vicinity of these lineaments could be prone to earth fissure formation, especially if the differential land subsidence worsens in the future.

Land-Surface Deformation Profiles

Vertical displacement interpreted using the InSAR interferograms is shown along profiles to show spatial heterogeneity over time for the study area (fig. 1). Negative vertical displacement values indicate subsidence, whereas positive values indicate uplift. Error of InSAR data, although minimized using techniques previously described, can be as much as 10 mm above or below the line of measurement shown in the profile. Comparison of geologic profile data with current InSAR data can be used to identify correlations between surface deformation and subsurface structure.

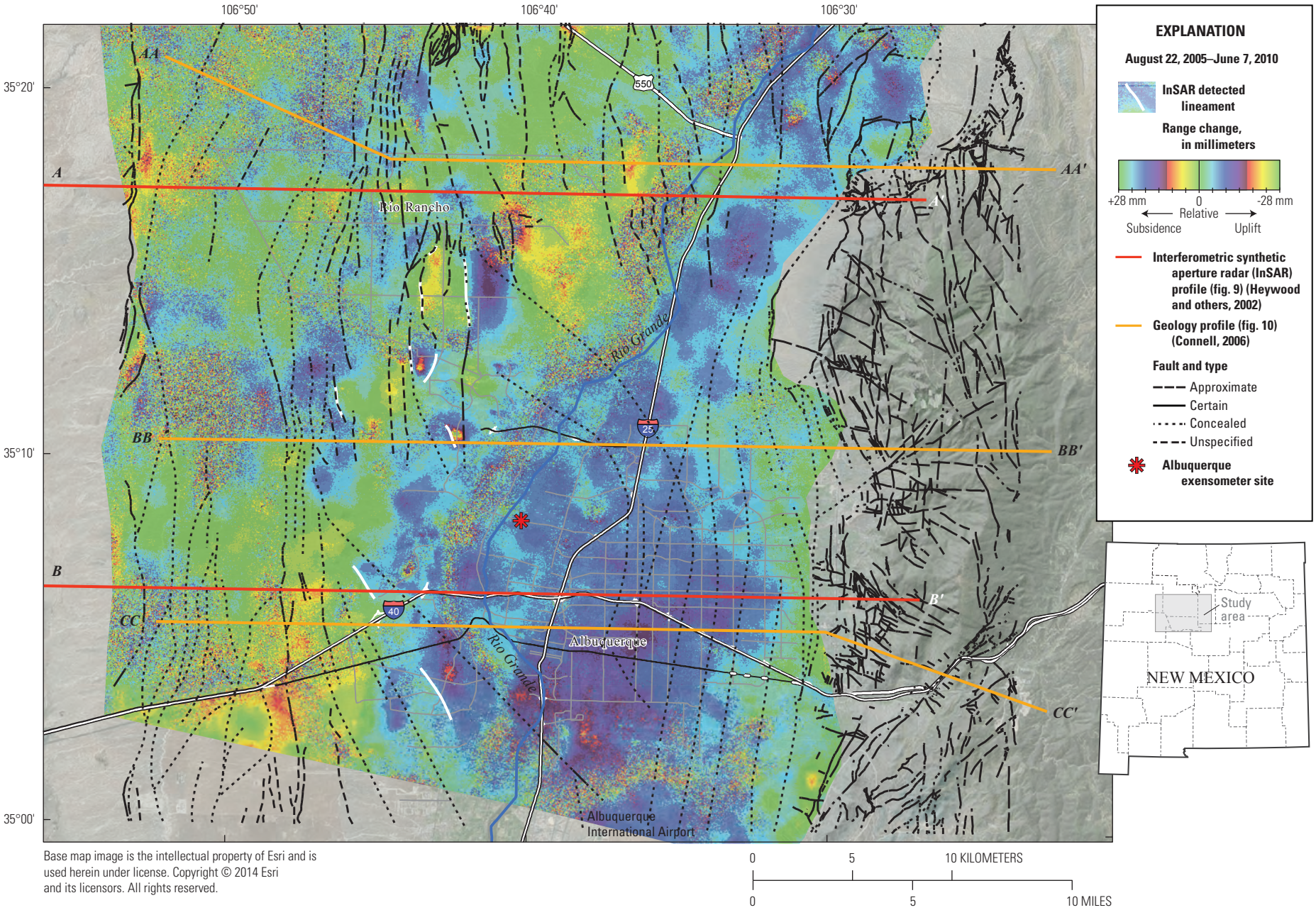

Figure 7. Composite interferogram for the Albuquerque Basin study area between August 22, 2005, and June 7, 2010 (1,750-day timespan).

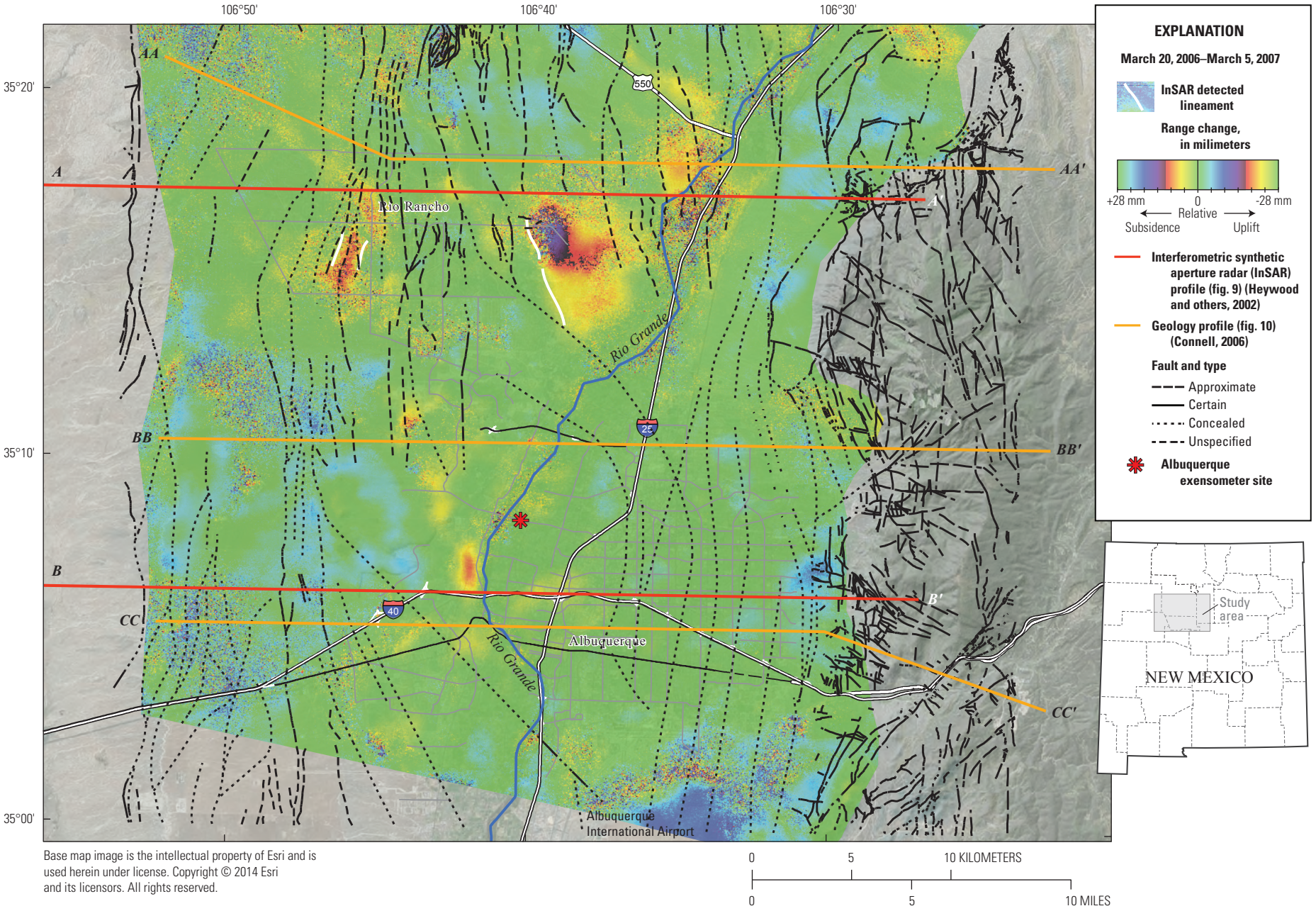

Figure 8*A*. Annual and seasonal interferograms of the Albuquerque Basin study area between *A*, March 20, 2006, and March 5, 2007; *B*, January 29, 2007, and February 18, 2008; *C*, November 5, 2007, and June 2, 2008; and *D*, July 7, 2008, and June 7, 2010. White lines are locations of InSAR detected lineaments that partially control the lateral extent of land deformation for each particular interferogram.

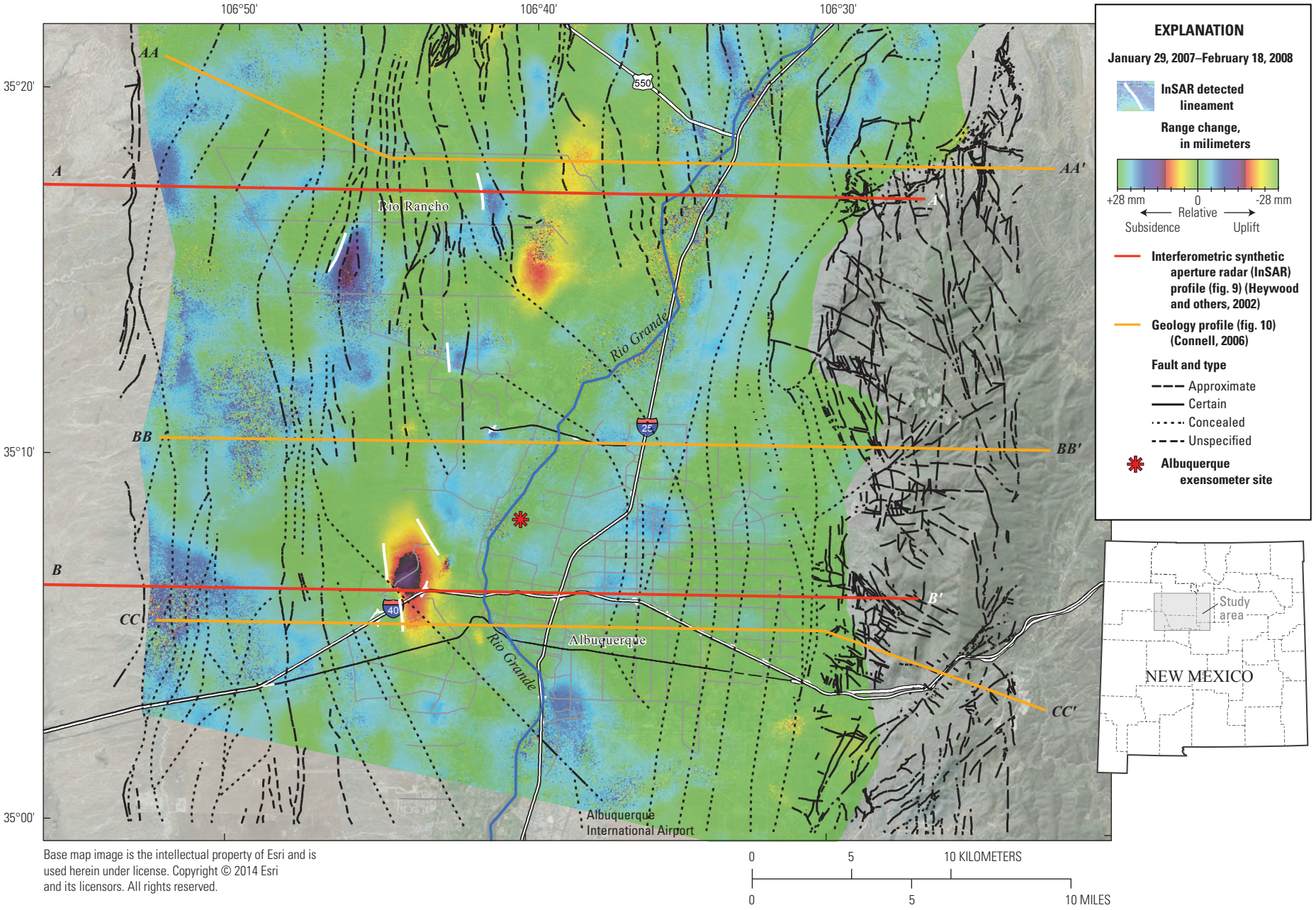

Figure 8*B*. Annual and seasonal interferograms of the Albuquerque Basin study area between *A*, March 20, 2006, and March 5, 2007; *B*, January 29, 2007, and February 18, 2008; *C*, November 5, 2007, and June 2, 2008; and *D*, July 7, 2008, and June 7, 2010. White lines are locations of InSAR detected lineaments that partially control the lateral extent of land deformation for each particular interferogram.

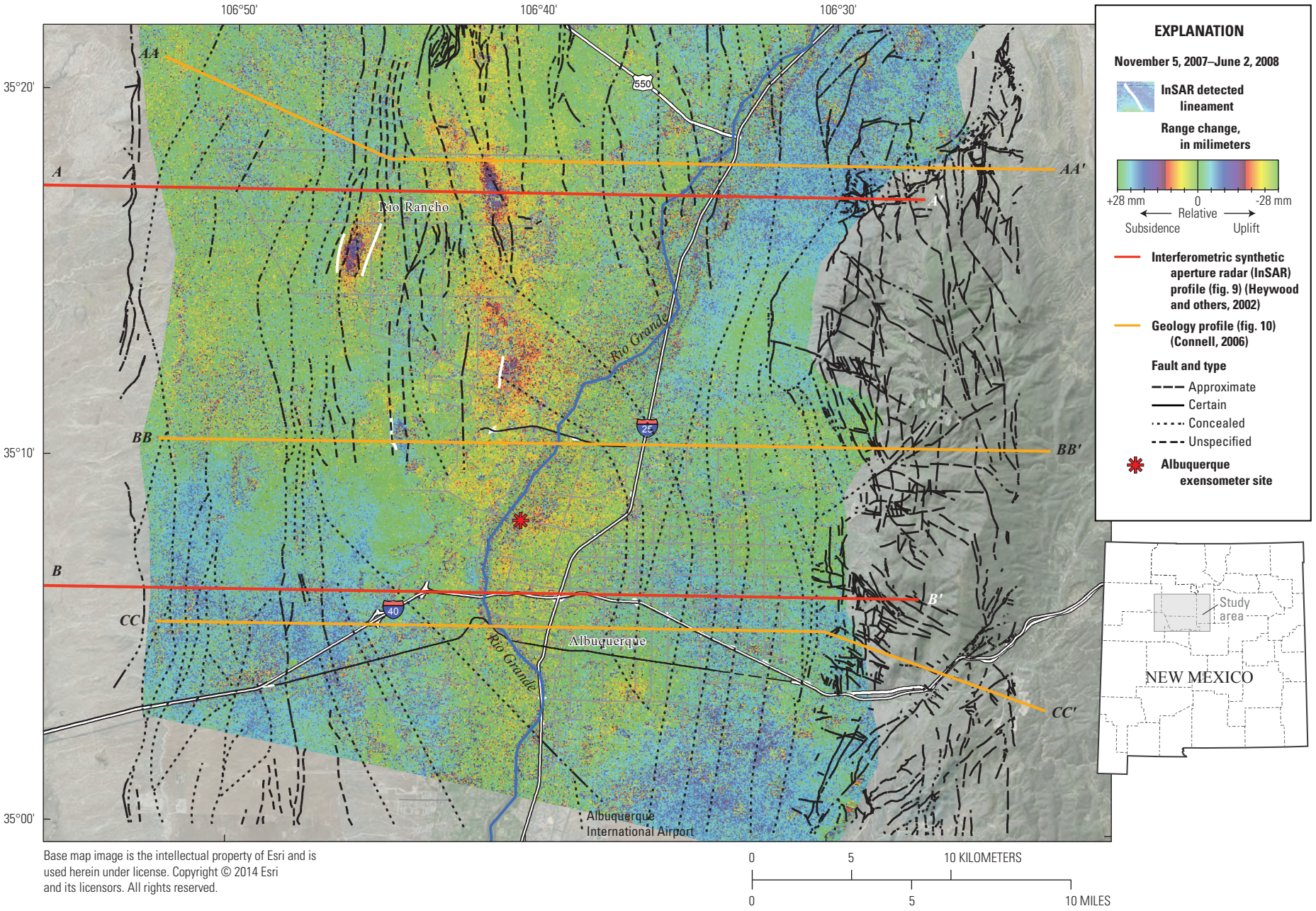

Figure 8*C*. Annual and seasonal interferograms of the Albuquerque Basin study area between *A*, March 20, 2006, and March 5, 2007; *B*, January 29, 2007, and February 18, 2008; *C*, November 5, 2007, and June 2, 2008; and *D*, July 7, 2008, and June 7, 2010. White lines are locations of InSAR detected lineaments that partially control the lateral extent of land deformation for each particular interferogram.

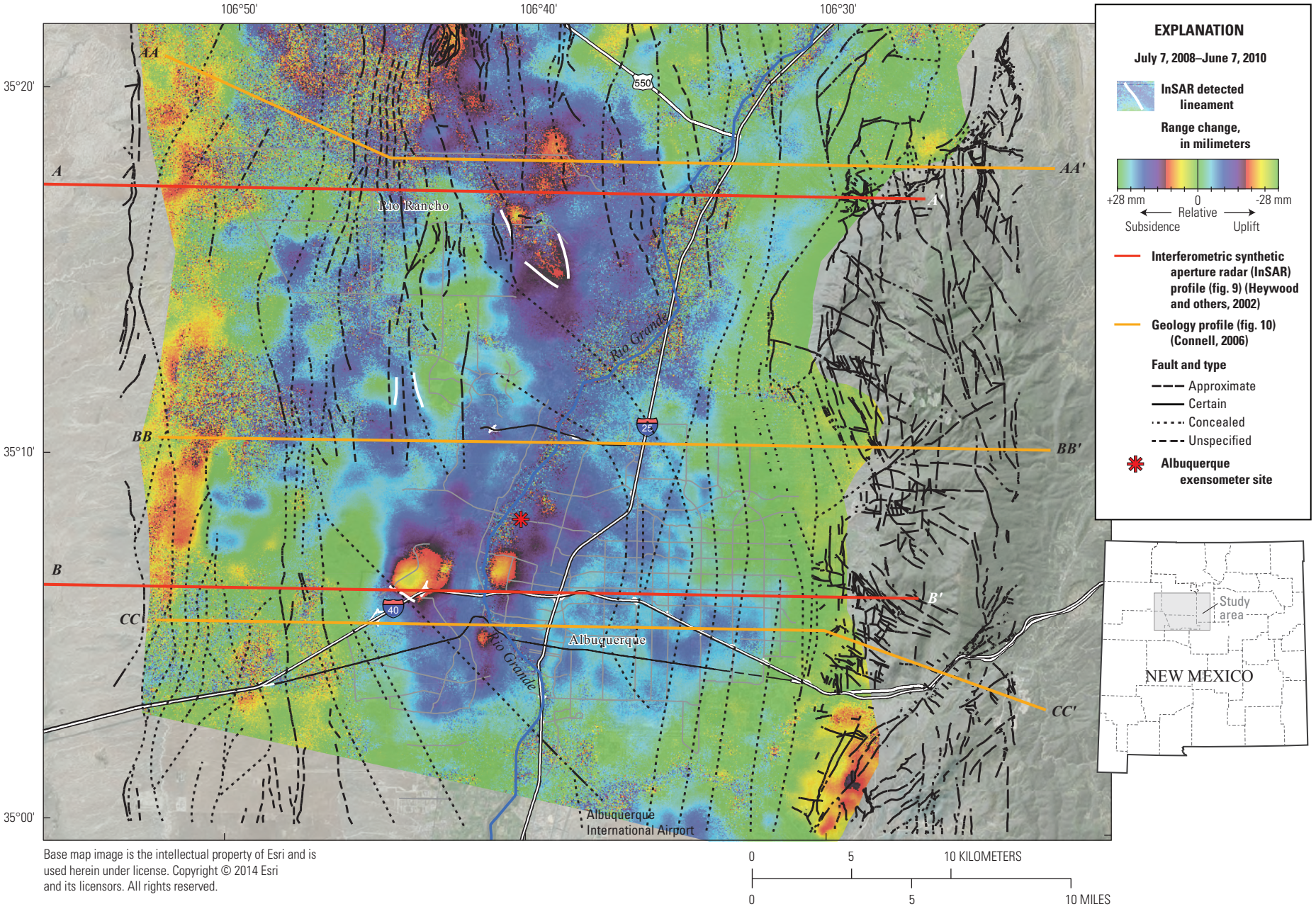

Figure 8*D*. Annual and seasonal interferograms of the Albuquerque Basin study area between *A*, March 20, 2006, and March 5, 2007; *B*, January 29, 2007, and February 18, 2008; *C*, November 5, 2007, and June 2, 2008; and *D*, July 7, 2008, and June 7, 2010. White lines are locations of InSAR detected lineaments that partially control the lateral extent of land deformation for each particular interferogram.

The locations of profiles were inherited from previous InSAR and geologic studies: two land-surface deformation profiles (*A–A'* and *B–B'*) were developed by Heywood and others (2002), and three geologic profiles (*AA–AA'*, *BB–BB'*, and *CC–CC'*) were developed by (Connell, 2006). Comparison of deformation profiles created from 1990s InSAR data (Heywood and others, 2002) with those created from 2005 to 2008 InSAR data permits deformation assessment of two before SJCDWP periods (fig. 9*A–B*), although profiles created from 2008 to 2010 InSAR data permit deformation assessment after SJCDWP (fig. 9*A–B*). Comparison of before SJCDWP and after SJCDWP deformation profiles can be used to identify changes in deformation trends that could be related to the SJCDWP.

Comparison of Land-Surface Deformation Profiles with Previous InSAR Profiles

Interferograms produced using SAR data for three multiannual periods (July 2, 1993–September 3, 1995; August 22, 2005–June 2, 2008; and July 7, 2008–June 7, 2010) were selected to create vertical displacement profiles along the same profiles as Heywood and others (2002), *A–A'* and *B–B'*. The SAR data used to produce these interferograms were acquired during annual or multiannual (similar season to similar season) or cross-seasonal (relative groundwater low to groundwater high) timeframes in order to capture long-term (annual or multiannual) and short-term (seasonal) deformation patterns. These deformation profiles run through the Rio Rancho metropolitan area (profile *A–A'*) and the Albuquerque metropolitan area (profile *B–B'*). The vertical displacement along both profiles for each time period shows spatial heterogeneity of land-surface elevation changes in the study area.

For the *A–A'* profile, the largest magnitude vertical displacement values are from the 1993–95 data (fig. 9*A*). The greatest negative vertical displacement along *A–A'* was measured at approximately 23 km from the west end of the profile (*A*), showing nearly 45 mm subsidence at this location for the 1993–95 time period. This same location showed no (zero mm) vertical displacement for the 2005–8 time period and uplift of approximately 5 mm vertical displacement for the 2008–10 time period. The largest positive vertical displacement along *A–A'* was measured at approximately 17 km from *A*, showing nearly 30 mm of uplift at this location for the 1993–95 time period. This same location showed less than 5 mm of subsidence for the 2005–8 and 2008–10 time periods. The profile along *A–A'* approximately 30 km from *A* (west of the Rio Grande) shows less than 5 mm of subsidence for the 1993–95 and 2005–8 time periods and approximately 8 mm of uplift during the 2008–10 time period.

Vertical displacement data along profile *B–B'* are of similar magnitudes for all three time periods and show less spatial heterogeneity relative to the vertical displacement data along *A–A'* (fig. 9*B*). The 1993–95 data along profile *B–B'* show negative vertical displacement west of the Rio Grande, with a localized subsidence of nearly 20 mm occurring about 21 km from *B* (about 3 km west of the Rio Grande). The 2005–8 time period shows a similar magnitude of negative vertical displacement west of the Rio Grande, and the 2008–10 data indicate about 20 mm of uplift occurred at this location. Profile *B–B'* also indicates that between 30 and 40 km from *B* (east of the Rio Grande) nearly 15 mm of subsidence occurred during the 1993–95 time period, whereas uplift occurred for the later time periods (15 mm and 5 mm of uplift for the 2005–8 and 2008–10 time periods, respectively) (fig. 9*B*).

Land-Surface Deformation Profiles Along Geology Profiles

Three land-surface deformation profiles (*AA–AA'*, *BB–BB'*, and *CC–CC'*) that correspond to geologic profiles developed by Connell (2006) were constructed for two time periods using InSAR measurements: (1) August 22, 2005–June 2, 2008, and (2) July 7, 2008–June 7, 2010 (figs. 1 and 10*A–C*). These time periods correspond approximately to before and after changes in municipal groundwater pumping related to the SJCDWP. These profile alignments permit comparisons of land-surface deformation with subsurface stratigraphy (fig. 10, available at https://doi.org/10.3133/sir20175057).

The 2005–8 InSAR data along profile *AA–AA'* indicate between 10 mm of uplift and 10 mm of subsidence between about 13 km (at the bend in the *AA–AA'* profile) and 28 km (at the Rio Grande), whereas the 2008–10 data indicate between 0 and 15 mm of uplift for the same locations. East of the Rio Grande, however, the 2005–8 InSAR data indicate between 5 and 10 mm of uplift, whereas the 2008–10 data indicate stability (fig. 10*A*). InSAR data along profile *BB–BB'* indicate similar deformation patterns for the area west of the Rio Grande for the 2005–8 and 2008–10 time periods. East of the Rio Grande, however, there is a general decrease in uplift magnitudes, and the 2005–8 InSAR data along this profile indicate a maximum of about 10 mm of uplift, and the 2008–10 data indicate no more than about 5 mm of uplift (fig. 10*B*). InSAR data for 2005–8 along profile *CC–CC'* indicate relative stability (less than about 5 mm of uplift or subsidence) between about 5 km from the western extent of the *CC–CC'* profile and the Rio Grande. The InSAR data indicate that most of the area between the Rio Grande and just west of Interstate 25 was stable for 2005–8, but about 5 to 10 mm of uplift were indicated for 2008–10. The area between Interstate 25 and the eastern terminus of the profile shows similar deformation patterns for 2005–8 and 2008–10, but the 2008–10 data show uplift of about 5 mm less as compared to 2005–8 data (fig. 10*C*).

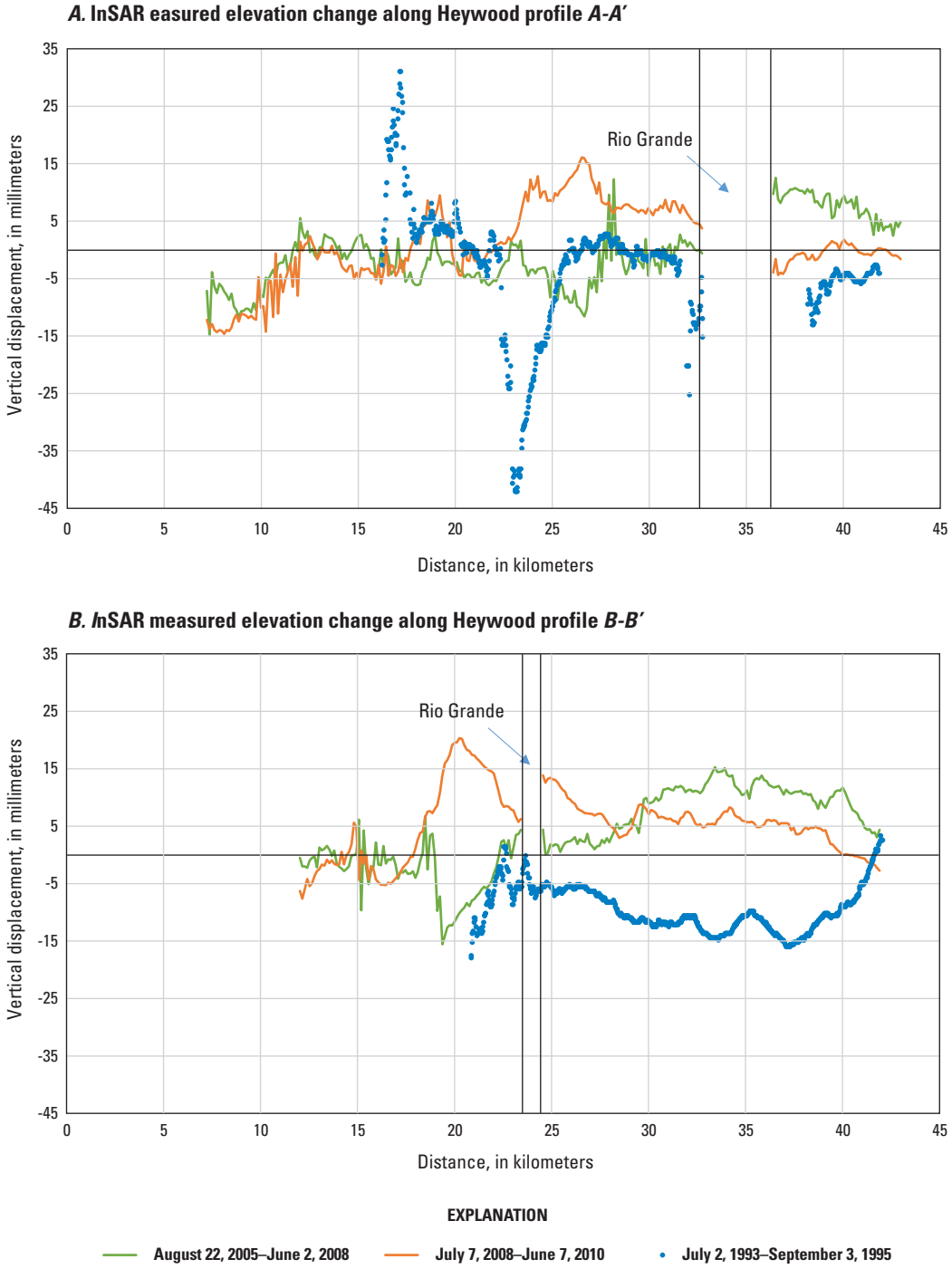

Figure 9. Interferometric Synthetic Aperture Radar (InSAR) land-surface elevation change from three interferogram time periods (1993–95, 2005–8, and 2008–10): *A*, along profile *A–A′*; and *B*, along profile *B–B′*. The 1993–95 InSAR data are from Heywood and others, 2002.

The groundwater table mapped along profile *CC–CC'* (Connell, 2006) provides an estimate for the depth to groundwater at that time. Although this representation of the groundwater table may not be precise, this estimate of the groundwater table relative to the stratigraphic units in which the groundwater table fluctuates may be related to the magnitude of deformation along the profiles. In areas where the clay-rich portions of the Atrisco Member (Tca) of the Ceja Formation are below the groundwater table, more deformation might be expected because of elastic and inelastic compaction than other sandier members of the Santa Fe Group. The variability of thicknesses and lateral continuity of each of these units, in addition to structural complexities such as faulting, may also influence the surface deformation in the area; however, there is a spatial relation along profile *CC–CC'* between where the estimated groundwater table occurs within the Tca and where InSAR data show little vertical displacement.. On the west side of the Albuquerque Basin (generally west of the Rio Grande), there is minimal difference between the two InSAR profiles in terms of vertical displacement where the groundwater table is within the Tca; in fact, both time periods show stability for this area. When the groundwater table is within the undivided deposits of the Ceja Formation (Tc), which contain more sands and gravels interbedded with finer-grained deposits, there is a greater difference between the two InSAR profiles (for example, between about 13 km from west end of the profile and the Rio Grande, fig. 10*C*); the post-SJCDWP profile shows between about 5 mm and 10 mm of uplift, indicating elastic recovery in this area. The spatiotemporal variability of the depth to groundwater in conjunction with the complexity of the subsurface stratigraphy makes comparison between patterns of deformation and the depth of the groundwater table difficult. Although this analysis is outside the scope of the present study, further analysis of the spatiotemporal variability of the potentiometric surface of groundwater, extent of subsurface clay-rich stratigraphy (and vertical thickness) and whether the fine-grained deposits occur as discontinuous interbeds or laterally extensive confining units, and land-surface elevation change could lead to better understanding the relation of each of these components.

Interferometric Synthetic Aperture Radar and Groundwater Levels

Groundwater levels in the Albuquerque Basin have recovered substantially since the SJCDWP reduced water supply production from wells in the area (Beman and Bryant, 2016). The InSAR time series were constructed at 10 locations where continuous water-level records were available (9 in Albuquerque and 1 in Rio Rancho) (fig. 11). These time series were constructed to facilitate a comparison of land-surface elevation changes to groundwater-level changes. It should be noted, however, that there are limitations with comparing InSAR measured deformation and changes in water levels. Water levels are measured in wells that generally have screens that are on the order of several meters long at specific depths, whereas InSAR measures the displacement of the land surface that would reflect the aggregate displacements (compaction or expansion) for the entire aquifer system and any displacement occurring in the underlying bedrock. For example, if aquifer-system compaction occurs at a depth that is not represented by the screened interval of a given well, the InSAR measured displacement may not correlate with changes in water levels recorded in that well.

Interferometric Synthetic Aperture Radar (InSAR) time series generally demonstrate correlations with available groundwater-level records. Ten wells with continuous data were selected to compare to InSAR data: Nor Este, Del Sol, Matheson, Montessa, West Bluff, Armijo2, Garfield, Sierra Vista, Westgate, and Lincoln (fig. 11; table 4). Groundwater-level data are available in the USGS NWIS at https://doi.org/10.5066/F7P55KJN.

Of these 10 selected well locations (fig. 1), 9 are within the Albuquerque metropolitan area (fig. 11*A–I*), and 1 is in the Rio Rancho metropolitan area (fig. 11*J*). Comparison with InSAR data at eight of these locations (Nor Este, Del Sol, Matheson, Montessa, West Bluff, Armijo2, Garfield, and Sierra Vista) indicates seasonally variable deformation and between 5 mm and 20 mm of longer term land-surface recovery (uplift) associated with groundwater-level recovery between 1 and 6 m from 2005 to 2010. One location, Westgate (fig. 11*I*), shows no land-surface deformation although about 3 m of groundwater-level recovery occurred. Lincoln, the Rio Rancho location, shows an uncertain correlation between the 1.5 m or less of groundwater-level decline and the relatively stable ground displacements during 2005–10 (fig. 11*J*).

Table 4. List of well names and U.S. Geological Survey identification numbers used for groundwater-level comparison to land-surface elevation data.

Well name	U.S. Geological Survey identification number	Data type
Montessa	350056106370102	Continuous
Westgate	350244106450202	Continuous
Armijo2	350307106410602	Continuous
Lincoln	351515106410402	Continuous
Nor Este	351114106330602	Continuous
Del Sol	350534106354702	Continuous
West Bluff	350638106413702	Continuous
Matheson	350653106311602	Continuous
Garfield	350706106390302	Continuous
Sierra Vista	350910106414802	Continuous

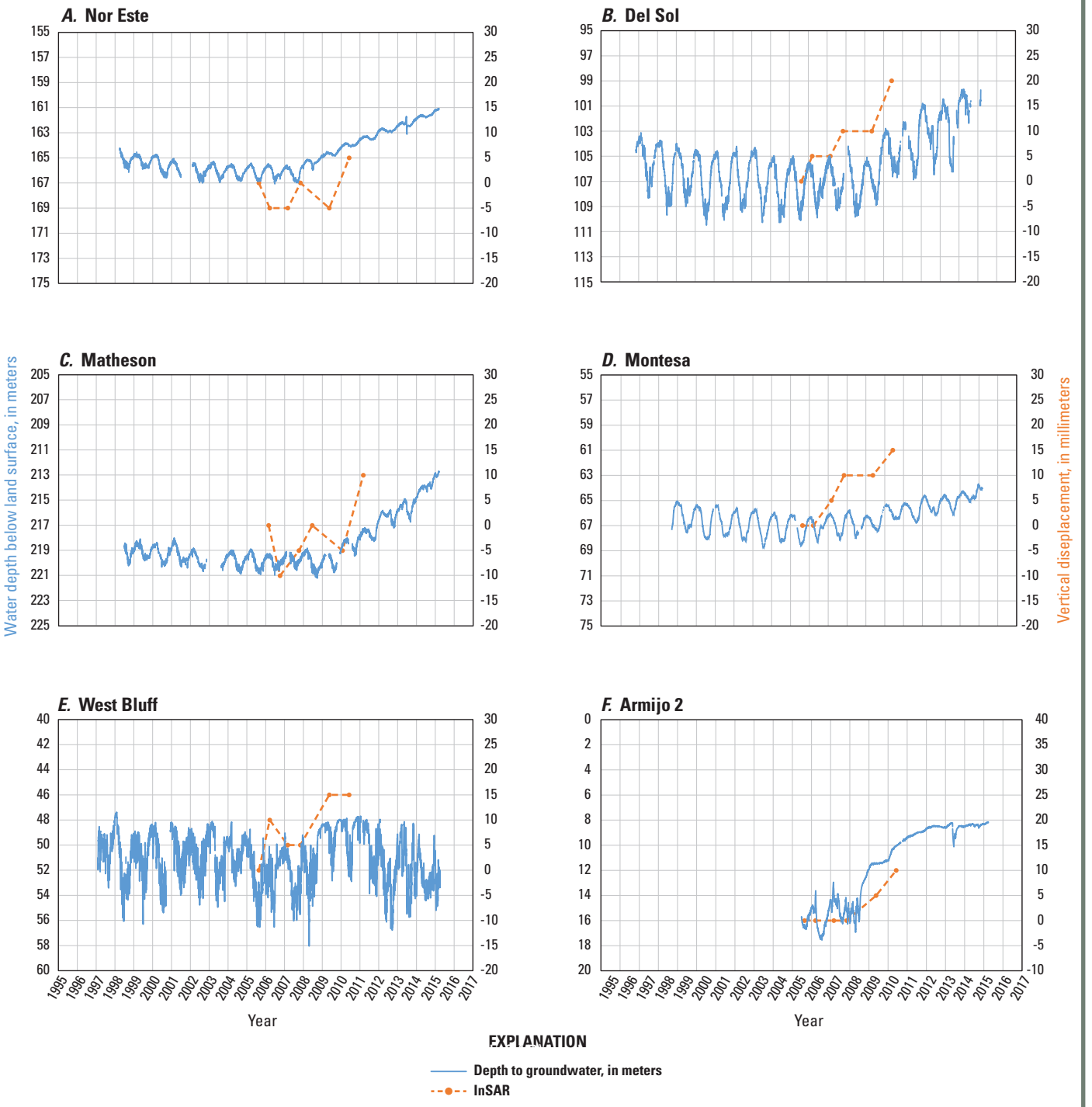

Figure 11. Continuous groundwater levels and Interferometric Synthetic Aperture Radar (InSAR) time series data.

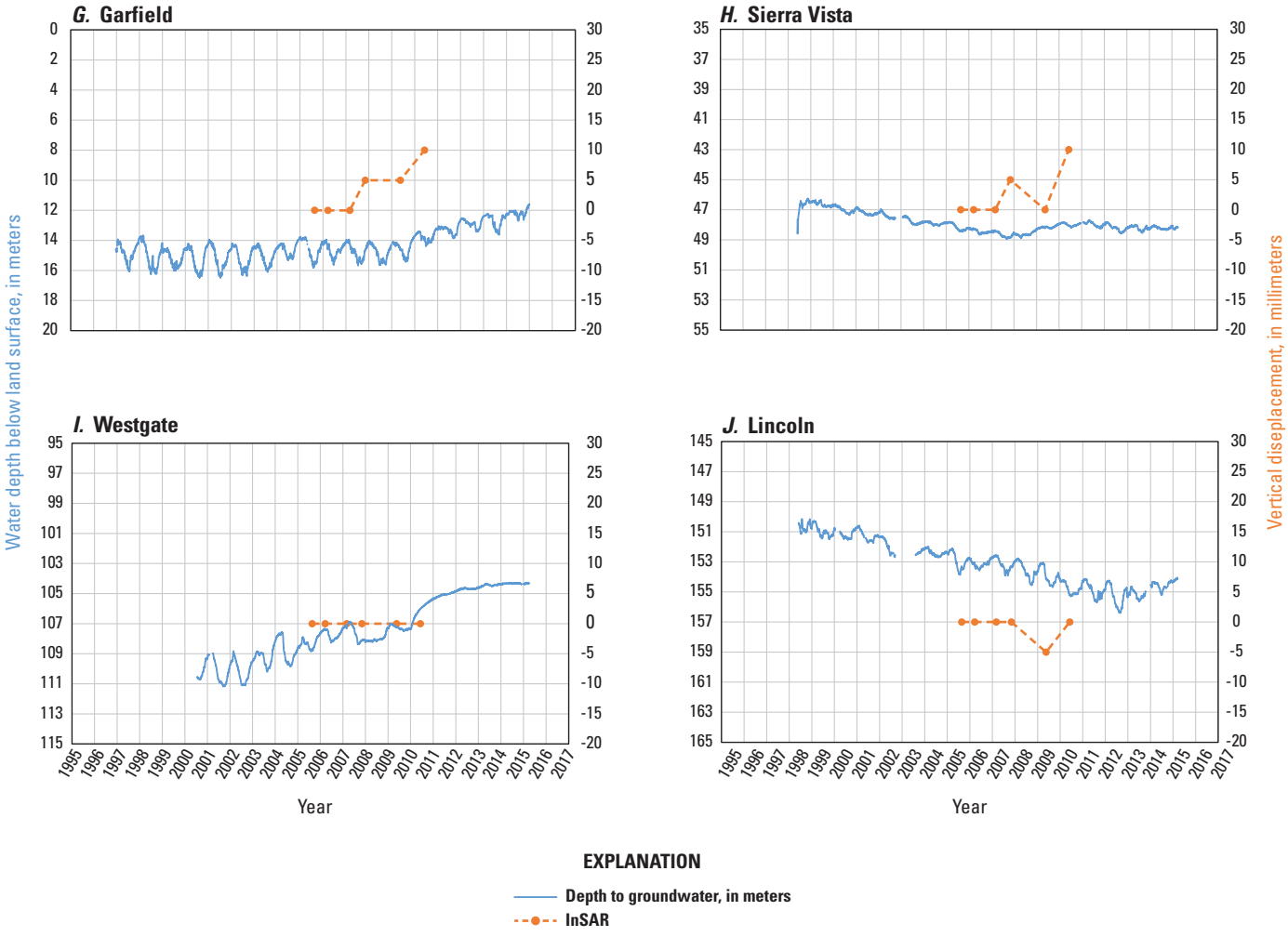

Figure 11. Continuous groundwater levels and Interferometric Synthetic Aperture Radar (InSAR) time series data—Continued.

Summary

The Albuquerque Bernalillo County Water Utility Authority (ABCWUA) drinking water supply was almost exclusively sourced from groundwater from within the Albuquerque Basin before 2008. The San Juan-Chama Drinking Water Project (SJCDWP) provided surface-water resources to augment the groundwater supply in 2008, allowing for a reduction in groundwater pumping in the Albuquerque Basin. Three methods of data collection and analysis with different temporal and spatial resolutions were used for this study: (1) aquifer-system compaction data collected continuously at a single extensometer from 1994 to 2013; (2) land-surface elevation change from Global Positioning System (GPS) surveys of a network of monuments collected in 1994–95, 2005, and 2014; and (3) spatially distributed Interferometric Synthetic Aperture Radar (InSAR) satellite data from 1993 to 2010. Extensometer data allow for direct and constant measurements of subsurface compaction, GPS surveys of monument networks provide a periodic update of land-surface elevation change at distributed locations, and interferograms provide greater spatial distribution of land-surface elevation change, which provide a landscape-scale understanding of land-surface elevation change over the Albuquerque Basin.

Results do not show substantial subsidence in the Albuquerque Basin. High temporal-resolution but low spatial resolution data measurements of aquifer-system compaction at the Albuquerque extensometer show elastic aquifer-system response to recovering groundwater levels. These point measures of aquifer-system compaction relative to the depth of groundwater show an overall reduction in elastic aquifer-system deformation when the SJCDWP reduced groundwater pumping, which led to groundwater-level recovery in 2008.

Results from GPS surveys of the Land-Subsidence Survey network of monuments show inconsistent land-surface elevation changes over the Albuquerque Basin. The inconsistency of direction of land-surface elevation change over time is likely because of the lack of substantial change and the complexity of subsurface stratigraphy in addition to the spatial and temporal heterogeneity of groundwater withdrawal over the study period.

Results from the InSAR analysis show areas of land-surface elevation increase after 2008, which could be attributed to elastic recovery of the aquifer system. The spatial extent to which elastic recovery of the aquifer system has resulted in recovery of land-surface elevation is limited to the in-situ measurements at the extensometer. Examination of spatially distributed InSAR data relative to limited spatial extent of the complex heterogeneity subsurface stratigraphy may explain some of the heterogeneity of land-surface elevation changes over this study period.

References Cited

Albuquerque Bernalillo County Water Utility Authority [ABCWUA], 2009, San Juan-Chama drinking water project—One-year anniversary: Albuquerque Bernalillo County Water Use Authority, 8 p., accessed November 5, 2014, at http://www.abcwua.org/education/pdfs/SJCDWPAnniversary.pdf.

Amelung, F., Galloway, D.L., Bell, J.W., Zebker, H.A., and Laczniak, R.J., 1999, Sensing the ups and downs of Las Vegas—InSAR reveals structural control of land subsidence and aquifer-system deformation: Geology, v. 27, no. 6, p. 483–486.

Bartolino, J.R., and Cole, J.C., 2002, Ground-water resources of the Middle Rio Grande Basin, New Mexico: U.S. Geological Survey Circular 1222, 132 p. [Also available at https://pubs.usgs.gov/circ/2002/circ1222/#pdf.]

Bell, J.W., and Helm, D.C., 1998, Ground cracks on Quaternary faults in Nevada—Hydraulic and tectonic, *in* Borchers, J.W., ed., Land subsidence case studies and current research: Proceedings of the Dr. Joseph F. Poland symposium on land subsidence: Association of Engineering Geologists Special Publication No. 8, p. 165–173.

Bell, J.W., Amelung, F., Ramelli, A.R., and Blewitt, G., 2002, Land subsidence in Las Vegas, Nevada, 1935–2000—New geodetic data show evolution, revised spatial patterns, and reduced rates: Environmental & Engineering Geoscience, v. VIII, no. 3, p. 155–174.

Beman, J.E., and Bryant, C.F., 2016, Water-level data for the Albuquerque Basin and adjacent areas, central New Mexico, period of record through September 30, 2015: U.S. Geological Survey Data Series 1025, 39 p., accessed January 6, 2017, at https://doi.org/10.3133/ds1025.

Bexfield, L.M., and Anderholm, S.K., 2002, Estimated water-level declines in the Santa Fe Group aquifer system in the Albuquerque area, central New Mexico, predevelopment to 2002: U.S. Geological Survey Water-Resources Investigations Report 2002–4233, 1 p., accessed October 20, 2014, at http://pubs.er.usgs.gov/publication/wri024233.

Connell, S.D., 2006, Geologic map of the Albuquerque-Rio Rancho metropolitan area and vicinity: New Mexico Bureau of Geology and Mineral Resources Geologic Map 78, accessed November 17, 2015, at https://geoinfo.nmt.edu/publications/openfile/details.cfml?volume=496.

Connell, S.D., Allen, B.D., and Hawley, J.W., 1998, Subsurface stratigraphy of the Santa Fe Group from borehole geophysical logs, Albuquerque area, New Mexico: New Mexico Geology, v. 20, no. 2, p. 7.

Contaldo, G.J., and Mueller, J.E., 1991a, Earth Fissures and Land Subsidence of the Mimbres Basin, Southwestern New Mexico, U.S.A., *in* Johnson, A.I., ed., Land subsidence—Proceedings of the Fourth International Symposium on Land Subsidence, May 12–17, 1991, Houston, Texas: International Association of Hydrological Sciences Publication 200, p. 301–310, accessed December 11, 2016, at http://hydrologie.org/redbooks/a200/iahs_200_0301.pdf.

Contaldo, G.J., and Mueller, J.E., 1991b, Earth fissures of the Mimbres Basin, Southwestern New Mexico: New Mexico Geology, v.13, no. 4, p. 69-74, accessed December 11, 2016, at https://geoinfo.nmt.edu/publications/periodicals/nmg/13/n4/nmg_v13_n4_p69.pdf.

Conway, B.D., 2016, Land subsidence and earth fissures in south-central and southern Arizona, USA: Hydrogeology Journal, v. 24, no. 3, p. 649-655, doi: 10.1007/s10040-015-1329-z.

Falk, S.E., Bexfield, L.M., and Anderholm, S.K., 2011, Estimated 2008 groundwater potentiometric surface and predevelopment to 2008 water-level change in the Santa Fe Group aquifer system in the Albuquerque area, central New Mexico: U.S. Geological Survey Scientific Investigations Map 3162, 1 sheet, accessed October 20, 2014, at http://pubs.usgs.gov/sim/3162/.

Fielding, E.J., Blom, R.G., and Goldstein, R.M., 1998, Rapid subsidence over oil fields measured by SAR interferometry: Geophysical Research Letters, v. 25, no. 17, p. 3215–3218.

Galloway, D.L., Hudnut, K.W., Ingebritsen, S.E., Phillips, S.P., Peltzer, G., Rogez, F., and Rosen, P.A., 1998, Detection of aquifer system compaction and land subsidence using interferometric synthetic aperture radar, Antelope Valley, Mojave Desert, California: Water Resources Research, v. 34, no. 10, p. 2573–2585.

Galloway, D.L., Jones, D.R., and Ingebritsen, S.E., eds., 1999, Land subsidence in the United States: U.S. Geological Survey Circular 1182, 165 p., accessed December 3, 2015, at http://pubs.usgs.gov/circ/circ1182/pdf/circ1182_intro.pdf.

Haneberg, W.C., and Friesen, R.L., 1995, Tilt and aquifer hydraulic-head changes near an earth fissure in the subsiding Mimbres Basin, New Mexico, *in* Prince, K.R., Galloway, D.L., and Leake, S.A., eds., U.S. Geological Survey Subsidence Interest Group Conference, Edwards Air Force Base, Antelope Valley, California, November 18-19, 1992: Abstracts and summary: U.S. Geological Survey Open-File Report 94-532, p. 59-62.

Hanson, R.T., 1989, Aquifer-system compaction, Tucson Basin and Avra Valley, Arizona: U.S. Geological Survey Water-Resources Investigations Report 88–4172, accessed November 16, 2015, at http://pubs.er.usgs.gov/publication/wri884172.

Hawley, J.W., 1994, An underground view of the Albuquerque Basin: New Mexico Water Resources Research Institute Report 290, p. 27–55, accessed January 20, 2017, at http://www.wrri.nmsu.edu/publish/watcon/proc39/Hawley.pdf.

Helm, D.C., 1978, Field verification of a one-dimensional mathematical model for transient compaction and expansion of a confined aquifer system—Verification of mathematical and physical models in hydraulic engineering: Proceedings 26th Hydraulic Division Specialty Conference, American Society of Civil Engineers, p. 189–196.

Helsel, D.R., and Hirsch, R.M., 2002, Statistical methods in water resources: U.S. Geological Survey Techniques of Water-Resources Investigations, book 4, chap. A3, 522 p.

Heywood, C.E., 1998, Piezometric-extensometric estimations of specific storage in the Albuquerque Basin, New Mexico, *in* Borchers, J.W., ed., Land subsidence case studies and current research: Proceedings of the Dr. Joseph F. Poland Symposium, Belmont, Calif., Star Publishing Company, p. 435–440.

Heywood, C.E., Galloway, D.L., and Stork, S.V., 2002, Ground displacements caused by aquifer-system water-level variations observed using interferometric synthetic aperture radar near Albuquerque, New Mexico: U.S. Geological Survey Water-Resources Investigations Report 2002–4235, 18 p., accessed November 5, 2014, at http://pubs.er.usgs.gov/publication/wri024235.

Hoffman, Jörn, Leake, S.A., Galloway, D.L., and Wilson, A.M., 2003, MODFLOW-2000 ground-water model—User guide to the subsidence and aquifer-system compaction (SUB) package: U.S. Geological Survey Open-File Report 03-233, 46 p., accessed December 10, 2016, at http://pubs.usgs.gov/of/2003/ofr03-233/.

Hoffmann, Jörn, Zebker, H.A., Galloway, D.L., and Amelung, F., 2001, Seasonal subsidence and rebound in Las Vegas Valley, Nevada, observed by Synthetic Aperture Radar Interferometry: Water Resources Research, v. 37, no. 6, p. 1551–1566.

Holzer, T.L., 1984, Ground failure induced by ground-water withdrawal from unconsolidated sediment, *in* Holzer, T.L., ed., Man-induced land subsidence: Geological Society of America Reviews in Engineering Geology, v. 6, p. 67–105.

Holzer, T.L., and Galloway, D.L., 2005, Impacts of land subsidence caused by withdrawal of underground fluids in the United States, in Ehlen, J., Haneberg, W.C., and Larson, R.A., eds., Humans as Geologic Agents: Boulder, Colorado, Geological Society of America Reviews in Engineering Geology, v. XVI, p. 87–99, doi: 10.1130/2005.4016(08).

Holzer, T.L., and Pampeyan, E.H., 1981, Earth fissures and localized differential subsidence: Water Resources Research, v. 17, no. 1, p. 223-227.

Ireland, R.L., Poland, J.F., and Riley, F.S., 1984, Land subsidence in the San Joaquin Valley, California, as of 1980: U.S. Geological Survey Professional Paper 437-I, 93 p.

Konikow, L.F., and Leake, S.A., 2014, Depletion and capture—Revisiting "The Source of Water Derived from Wells": Groundwater, v. 52, no. S1, p. 100–111.

Leake, S.A., and Prudic, D.E., 1988, Documentation of a computer program to simulate aquifer-system compaction using the modular finite-difference ground-water flow model: U.S. Geological Survey, Open-File Report 88–482, 80 p., accessed November 16, 2015, at http://pubs.er.usgs.gov/publication/ofr88482.

Lund, W.R., DuRoss, C.B., Kirby, S.M., McDonald, G.N., and Hunt, G., 2005, The origin and extent of earth fissures in Escalante Valley, southern Escalante Desert, Iron County, Utah: Utah Geological Survey Special Study 115, 30 p., compact disk.

Massonnet, D., Briole, P., and Arnaud, A., 1995, Deflation of Mount Etna monitored by spaceborne radar interferometry: Nature, v. 375, no. 6532, p. 567–570.

Massonnet, D., Holzer, T., and Vadon, H., 1997, Land subsidence caused by the East Mesa Geothermal Field, California, observed using SAR interferometry: Geophysical Research Letters, v. 24, no. 8, p. 901–904.

Massonnet, D., Rossi, M., Carmona, C., Adranga, F., Peltzer, G., Feigl, K., and Rabaute, T., 1993, The displacement field of the Landers earthquake mapped by radar interferometry: Nature, v. 364, p. 138–142.

McAda, D.P., and Barroll, P., 2002, Simulation of ground-water flow in the Middle Rio Grande Basin between Cochiti and San Acacia, New Mexico: U.S. Geological Survey Water-Resources Investigations Report 2002–4200, 81 p., accessed September 17, 2015, at http://pubs.er.usgs.gov/publication/wri20024200.

Meinzer, O.E., 1928, Compressibility and elasticity of artesian aquifers: Economic Geology, v. 23, no. 3, p. 263–291.

Poland, J.F., 1984, Guidebook to studies of land subsidence due to groundwater withdrawal: Paris, France, United Nations Educational, Scientific and Cultural Organization Studies and Reports in Hydrology, 305 p., 5 appendices.

Powell, R.I., and McKean, S.E., 2014, Estimated 2012 groundwater potentiometric surface and drawdown from predevelopment to 2012 in the Santa Fe Group aquifer system in the Albuquerque metropolitan area, central New Mexico: U.S. Geological Survey Scientific Investigations Map 3301, 1 sheet, accessed October 15, 2014, at http://pubs.usgs.gov/sim/3301/.

Prince, K.R., and Leake, S.A., 1997, U.S. Geological Survey Subsidence Interest Group Conference, proceedings of the technical meeting, Las Vegas, Nevada, February 14-16, 1995: U.S. Geological Survey Open-File Report 97–47, 37 p., accessed November 17, 2015, at http://pubs.er.usgs.gov/publication/ofr9747.

Riley, F.S., 1969, Analysis of borehole extensometer data from central California, *in* Tison, L.J., ed., Land subsidence, volume 2: Proceedings of the Tokyo Symposium, September 1969: International Association of Scientific Hydrology Publication 89, p. 423–431, accessed November 16, 2015, at http://iahs.info/redbooks/a088/088047.pdf.

Riley, F.S., 1998, Mechanics of aquifer systems—The scientific legacy of Joseph F. Poland: Land Subsidence—Case Studies and Current Research: Proceedings of the Dr. Joseph F. Poland Symposium on Land Subsidence, Association of Engineering Geologists Special Publication 8, p. 13–27.

Schmidt, D.A., and Bürgmann, R., 2003, Time-dependent land uplift and subsidence in the Santa Clara Valley, California, from a large interferometric synthetic aperture radar data set: Journal of Geophysical Research, v. 108, no. B9.

Sneed, Michelle, and Brandt, J.T., 2007, Detection and measurement of land subsidence using Global Positioning System surveying and Interferometric Synthetic Aperture Radar, Coachella Valley, California, 1996–2005: U.S. Geological Survey Scientific Investigations Report 2007–5251, 31 p., accessed November 16, 2015, at http://pubs.er.usgs.gov/publication/sir20075251.

Sneed, Michelle, Brandt, Justin, and Solt, Mike, 2013, Land subsidence along the Delta-Mendota Canal in the northern part of the San Joaquin Valley, California, 2003–10: U.S. Geological Survey Scientific Investigations Report 2013–5142, 100 p., accessed November 16, 2015, at http://pubs.er.usgs.gov/publication/sir20135142.

Sneed, Michelle, Brandt, J.T., and Solt, Mike, 2014, Land subsidence, groundwater levels, and geology in the Coachella Valley, California, 1993–2010: U.S. Geological Survey Scientific Investigations Report 2014–5075, 62 p., accessed November 5, 2014, at http://pubs.usgs.gov/sir/2014/5075.

Sneed, Michelle, and Galloway, D.L., 2000, Aquifer-system compaction and land subsidence: measurements, analyses, and simulations—The Holly site, Edwards Air Force Base, Antelope Valley, California: U.S. Geological Survey Water-Resources Investigations Report 2000–4015, 65 p., accessed November 16, 2015, at http://pubs.er.usgs.gov/publication/wri20004015.

Terzaghi, K., 1925, Principles of soil mechanics, IV—Settlement and consolidation of clay: Engineering News-Record, p. 874–878.

Thorn, C.R., McAda, D.P., and Kernodle, J.M., 1993, Geohydrologic framework and hydrologic conditions in the Albuquerque Basin, central New Mexico: U.S. Geological Survey Water-Resources Investigations Report 93–4149, 106 p., accessed September 17, 2015, at http://pubs.er.usgs.gov/publication/wri934149.

University Navigation Satellite Timing and Ranging Consortium [UNAVCO], 2015, Station P034, unfiltered data with NAM08 reference frame, accessed May 4, 2015, at https://www.unavco.org/instrumentation/networks/status/pbo/data/P034.

Wilke, C., 2007, Albuquerque Basin subsidence monitoring network (2005): City of Albuquerque, 24 p.

Zebker, H.A., Rosen, P.A., and Hensley, S., 1997, Atmospheric effects in interferometric synthetic aperture radar surface deformation and topographic maps: Journal of Geophysical Research: Solid Earth, v. 102, no. B4, p. 7547–7563.

For more information about this publication, contact:
Director
U.S. Geological Survey
New Mexico Water Science Center
6700 Edith Blvd NE
Albuquerque, NM 87113

For additional information visit https://nm.water.usgs.gov/

Publishing support provided by:
Lafayette Publishing Service Center

ISSN 2328-0328 (online)
https://doi.org/ 10.3133/sir20175057